LAWRENCE
LIVERMORE
NATIONAL
LABORATORY

LLNL-JRNL-423303

Indirect and Semi-Direct Aerosol Campaign (ISDAC): The Impact of Arctic Aerosols on Clouds

G. M. McFarquhar, S. Ghan, J. Verlinde, A. Korolev, J. W. Strapp, B. Schmid, J. Tomlinson, M. Wolde, S. D. Brooks, D. Cziczo, M. K. Dubey, J. Fan, C. Flynn, I. Gultepe, J. Hubbe, M. K. Gilles, A. Laskin, P. Lawson, R. Leaitch, P. Liu, X. Liu, D. Lubin, C. Mazzoleni, A. M. Macdonald, R. C. Moffet, H. Morrison, M. Ovchinnikov, D. Ronfeld, M. Shupe, D. Turner, S. Xie, A. Zelenyuk, K. Bae, M. Freer, A. Glen

February 8, 2010

Bulletin of the American Meteorological Society

Disclaimer

Indirect and Semi-Direct Aerosol Campaign (ISDAC): The Impact of Arctic Aerosols on Clouds

Greg M. McFarquhar[1*], Steven Ghan[2], Johannes Verlinde[3], Alexei Korolev[4], J. Walter Strapp[4], Beat Schmid[2], Jason Tomlinson[2], Mengistu Wolde[5], Sarah D. Brooks[6], Dan Cziczo[2], Manvendra K. Dubey[7], Jiwen Fan[2], Connor Flynn[2], Ismail Gultepe[4], John Hubbe[2], Mary K. Gilles[8], Alexander Laskin[2], Paul Lawson[9], Richard Leaitch[4], Peter Liu[4], Xiaohong Liu[2], Dan Lubin[10], Claudio Mazzoleni[7&], Ann-Marie Macdonald[4], Ryan C. Moffet[8], Hugh Morrison[11], Mikhail Ovchinnikov[2], Debbie Ronfeld[2], Matthew D. Shupe[12], David D. Turner[13], Shaocheng Xie[14], Alla Zelenyuk[2], Kenny Bae[1], Matt Freer[1+] and Andrew Glen[6]

[1]University of Illinois, Illinois, USA
[2]Pacific Northwest National Laboratory, Richland, WA
[3]Penn State University, State Park, PA
[4]Science and Technology Branch, Environment Canada, Downsview, Canada
[5]National Research Council of Canada, Ottawa, Canada
[6]Texas A&M University, College Station, TX
[7]Los Alamos National Laboratory, Los Alamos, NM
[8]Lawrence Berkeley National Laboratory, Berkeley, CA
[9]Stratton Park Engineering Company, Boulder, CO
[10]Scripps Institution of Oceanography, La Jolla, CA
[11]National Center for Atmospheric Research, Boulder, CO
[123] Cooperative Institute for Research in Environmental Science, University of Colorado/NOAA, Boulder, CO
[13]University of Wisconsin, Madison, WI
[14]Lawrence Livermore National Laboratory, Livermore, CA
[+] Current Affiliation: European Facility for Airborne Research, Toulouse, France
[&]Current Affiliation: Michigan Technological University, Houghton, MI

Submitted to *Bull. Amer. Meteor. Soc.*, February 2010

*Corresponding Author: Dr. Greg M. McFarquhar, University of Illinois, Dept. of Atmospheric Sciences, 105 S. Gregory St., Urbana, IL, 61801-3070.

Capsule Summary

Preliminary scientific findings about cloud and aerosol processes in arctic mixed-phase clouds are described using an unique set of data collected during the Indirect and Semi-Direct Aerosol Campaign (ISDAC) are described.

Abstract

A comprehensive dataset of microphysical and radiative properties of aerosols and clouds in the arctic boundary layer in the vicinity of Barrow, Alaska was collected in April 2008 during the Indirect and Semi-Direct Aerosol Campaign (ISDAC) sponsored by the Department of Energy Atmospheric Radiation Measurement (ARM) and Atmospheric Science Programs. The primary aim of ISDAC was to examine effects of aerosols on clouds that contain both liquid and ice water for clean and polluted environments. ISDAC utilized the ARM permanent observational facilities at Barrow. These include a cloud radar, a polarized micropulse lidar, and an atmospheric emitted radiance interferometer as well as instruments specially deployed for ISDAC measuring aerosol, ice fog, precipitation and spectral shortwave radiation. The National Research Council of Canada Convair-580 flew 27 sorties during ISDAC, collecting data using an unprecedented 42 state-of-the-art cloud and aerosol instruments for more than 100 hours on 12 different days. Data were obtained on a number of days, including above, below and within single-layer stratus on 8 April and 26 April 2008. These data enable a process-oriented understanding of how aerosols affect the microphysical and radiative properties of arctic clouds influenced by different surface conditions and aerosol loads. Observations acquired on a heavily polluted day, 19 April 2008, are enhancing this understanding. Data acquired in cirrus on transit flights between Fairbanks and Barrow are improving our understanding of the performance of cloud probes in ice. Ultimately the ISDAC data will be used to improve the representation of cloud and aerosol processes in models covering a variety of spatial and temporal scales and pollution regimes, and to determine the extent to which long-term surface-based measurements can provide retrievals of aerosols, clouds, precipitation and radiative heating in the Arctic.

1. Introduction

Recent studies (ACIA 2005) concluded that the Arctic is warming twice as fast as the rest of the Earth, resulting in a rapid retreat of the arctic sea-ice. In September 2007, sea-ice extent was the smallest since satellite observations began in 1979 (Comiso et al. 2008). The observed sea ice melting and polar amplification of the warming exceeds expectations based on model simulations of the climate response to increasing greenhouse gas concentrations (IPCC 2007). Although snow and ice albedo feedbacks are likely primary drivers for the polar amplification (Vavrus 2004), other forcing and feedback mechanisms might also play important roles. In particular, climate model simulations suggest that cloud feedback (Vavrus 2004) and absorption by black carbon aerosol (Quinn et al. 2008) are important contributors to arctic warming. Indeed, observations show that changes in cloud properties may have played a significant role in the large sea ice loss during 2007 (Kay and Gettelman 2009). However, the uncertainty associated with the treatment of clouds and aerosols in climate models leads to much uncertainty in predictions of arctic climate change (Inoue et al. 2006). Thus, projections from state-of-the-art climate models range from the summer sea ice vanishing within 30 years (Wang and Overland 2009) to the end of the twenty-first century (Boe et al. 2009), with most models significantly underestimating the observed trend in arctic ice seasonal decline (Stroeve et al. 2007).

The complex interaction between clouds, aerosols and other components of the arctic climate system must be better understood in order to constrain large disagreements between global climate model (GCM) simulations of arctic temperature change. Observations show that clouds have an annual-mean net warming effect on the arctic surface (Walsh and Chapman 1998). However, GCM simulations and radiative transfer calculations show this effect is sensitive to assumed

cloud properties: for instance, modifying the effective radius of water droplets can alter the surface energy budget by up to 40 W m^{-2} (Curry et al. 1993) and a change in effective radius of ice crystals can induce variations up to 80 W m^{-2} (Harrington and Olsson 2001).

Field measurements provide the basis for improved understanding and representation of arctic cloud and aerosol processes in GCMs. Data collected at the Department of Energy Atmospheric Radiation Measurement (DOE ARM) Program's permanent ground-based facility at the North Slope of Alaska (NSA) show that mixed-phase (liquid and ice) clouds prevail in the spring and fall (Intrieri et al. 2002), meaning that water and ice co-exist. These clouds have a significant impact on the radiative budget (e.g., Dong et al. 2001) and occur in both single and multiple layers (Verlinde et al. 2007), with a typical layer structure having liquid tops and precipitating ice (Hobbs and Rangno 1998).

Arctic mixed-phase clouds can persist for days (Shupe et al. 2006). Modelling studies suggest they persist due to a balance between cloud top radiative cooling, latent heating, ice sedimentation and large-scale forcing (Pinto 1998; Harrington et al., 1999). This balance depends on assumptions about ice fall speeds, cloud single-scattering properties, ice nuclei concentrations, primary and secondary nucleation mechanisms and large scale forcing (e.g., Jiang et al. 2000). Fridlind et al. (2007) showed that the observed ambient ice nuclei (IN) were insufficient to explain the observed ice crystal concentrations and hypothesized that formation of ice nuclei from drop evaporation residuals and drop freezing during evaporation might explain the observed data. Sednev et al. (2008) suggested that the Bergeron-Findeisen process could account for the observations. However, because these studies were based on observations acquired in pristine conditions during the Mixed-Phase Arctic Cloud

Experiment (M-PACE) and because the response of arctic clouds to increased aerosols depends on the underlying surface conditions (Morrison et al. 2008), there is still a need to know how aerosols impact arctic clouds in a variety of aerosol, surface, and meteorological conditions.

There are considerable variations in the concentrations and composition of aerosols in the Arctic. Shaw (1982) first identified the arctic haze associated with the transport of anthropogenic pollutants from Europe and Asia. Aerosols are typically found in stratified layers at altitudes up to 9 km (Barrie 1986). A strong seasonal cycle has been observed over the NSA (Quinn et al. 2002) with the greatest aerosol concentrations found during winter and a marked transition between March and May as pollution events become rarer and clouds more frequent and thick. An examination of prior observations also suggests that higher cloud condensation nuclei (CCN) numbers occur in winter and early spring than in summer or early autumn (Leaitch et al. 1984; Yu and Hudson 2001), and that ice nuclei (IN) occur less frequently in October (Prenni et al. 2008) than in May (Rogers et al. 2001). The seasonal variations in nuclei concentrations are expected to produce seasonal variations in droplet and crystal concentrations, and long-term trends in aerosol could produce trends in cloud properties. The influence of these changes in cloud microphysical properties on solar radiation (known as the aerosol indirect effect on energy balance) is dominant in summer. Nevertheless variations in aerosol properties are still important because a longwave indirect effect in which higher drop numbers and smaller sizes increase longwave emissivity of clouds in the Arctic has been noted during winter months (Garrett and Zhao 2006; Lubin and Vogelmann 2006).

Black carbon has been found in at least some aerosols sampled at the ground in Barrow (Hansen et al., 1989) and by aircraft in Svalbard Norway (Hara et al. 2003).

Arctic climate is sensitive to black carbon because it affects snow albedo, accelerates melting (McConnell et al., 2007), and can lead to the evaporation of low-level clouds, the aerosol semi-direct effect on energy balance. Shindell and Faluvegi (2009) found that up to 70% of Arctic warming since 1976 could be accounted for by increased black carbon emissions. Thus, there is a need to identify the vertical distribution, composition and concentration of aerosols for studies of aerosol-cloud interactions.

Most prior studies of aerosol effects on clouds and radiation examined liquid clouds. Although some satellite studies have examined changes in ice crystal sizes due to increases in aerosols (Sherwood 2002), there are few studies of aerosol influences on mixed-phase clouds, particularly from a coordinated in-situ/remote sensing perspective. Because phase affects cloud radiative properties (e.g., Sun and Shine 2004), large eddy simulations (LES), cloud resolving models (CRMs) and GCMs must correctly treat aerosol effects on clouds with a variety of phases to determine radiative effects. Since recent modeling studies (Klein et al. 2009; Morrison et al. 2009) have shown that more sophisticated representations of cloud microphysics tend to produce simulations more consistent with observations, there is need for coordinated aerosol/cloud observations to develop and test model parameterizations. Prior field campaigns studying arctic clouds, such as the Surface Heat Budget of Arctic Ocean Experiment (SHEBA, Uttal et al., 2002), the First International Satellite Cloud Climatology Project (ISCCP) Regional Experiment Arctic Cloud Experiment (FIRE ACE, Curry et al., 2000), and M-PACE (Verlinde et al., 2007) provide some aerosol information, but single particle analysis of molecular composition was missing. A comprehensive cloud and aerosol data set is needed, particularly during the early spring when aerosol concentrations are high and sunlight is available to influence the arctic energy balance.

Three coordinated field experiments conducted over Alaska during April of the International Polar Year (2008) provided such data. The Indirect and Semi-Direct Aerosol Campaign (ISDAC) is the focus of this manuscript. The Arctic Research of the Composition of the Troposphere from Aircraft and Satellites Experiment (ARCTAS, Jacob et al., 2009) and the Aerosol, Radiation and Cloud Processes affecting the Arctic Experiment (ARCPAS, Warneke et al., 2009) were conducted at the same time as ISDAC and also contribute to this database.

This article provides an overview of ISDAC. The primary goal of ISDAC was to improve our knowledge on how changes in the composition and concentration of aerosols influence cloud properties and the associated radiative forcing. ISDAC, conducted in April 2008, built upon the success of M-PACE, conducted in October 2004, by allowing arctic aerosol and cloud properties to be contrasted between the relatively pristine fall and more polluted spring seasons. The National Research Council (NRC) of Canada Convair-580 flew 27 sorties (and 12 other transits and test flights), collecting data from an unprecedented 42 cloud and aerosol instruments for more than 100 hours on 12 different days in varying aerosol, surface and meteorological conditions. Flight plans were devised such that sampling was conducted above, below and at varying altitudes in cloud so that the data could be used for both process-oriented and statistical analysis.

The primary science questions addressed by ISDAC are listed in Table 1. A general theme was to provide detailed observations of aerosols and clouds. The ultimate goal of the Office of Biological and Environmental Research (BER) of the Office of Science in DOE is to deliver improved scientific data and models describing the potential response of the Earth's climate to increased greenhouse gas levels. Therefore ISDAC was designed to gather high quality data needed to improve the

treatment of clouds and aerosols in climate models. Another important component was to provide data for evaluating ground and space borne remotely sensed cloud, aerosol, precipitation and radiation profiles: these tie ISDAC to long-term observational data sets at the NSA site in Barrow.

2. Ground Network Observations

ARM has maintained a permanent observational site at the NSA (71°19'N and 156°37'W) since 1997. The NSA site was established because of the rapid changes occurring in the arctic environment and the large climate sensitivity due to the snow/ice albedo feedback. The site includes measurements of the surface radiation budget, surface meteorology and the vertical distribution of clouds (Table 2).

Cloud profiles are derived primarily from a vertically pointing 35 GHz cloud radar and a micropulse cloud lidar. In addition to cloud occurrence, these instruments provide profiles of cloud microphysical properties through various retrieval algorithms (e.g., Shupe et al. 2005). Other instruments such as the Atmospheric Emitted Radiance Interferometer (AERI), a microwave radiometer and a Multifilter Rotating Shadowband Radiometer (MFRSR) are used to derive cloud properties integrated over the entire column (e.g., Turner 2005, Turner et al. 2007, and Min and Harrison 1996, respectively). A Total Sky Imager allows determination of the fraction of the sky covered by clouds during daytime hours. Several radiometers measure upwelling and downwelling irradiances. Surface and tower meteorological instrumentation, a balloon borne sounding system and a radar wind profiler provide profiles of temperature, dew-point and winds.

In addition to the permanent instrumentation at the NSA, additional instruments were deployed for ISDAC. These included a shortwave spectroradiometer operating between 350 and 2200 nm with a resolution of 3 (10) nm in the visible/near-

infrared useful for retrieving cloud optical depth (τ) and effective radius. A tandem differential mobility analyser (TDMA) was used for measuring the size distribution of aerosol number and hygroscopicity in the diameter range between 0.01 and 0.6 μm. Ice fog and precipitation microphysical characteristics were measured by a Droplet Measurement Technologies (DMT) fog measuring device (FMD), a total precipitation sensor (TPS), a precipitation weighing sensor (VRG101), and disdrometers. Table 2 summarizes the operating characteristics of the ground-based instruments, and Figure 1 is a photograph of the ground-based facility at Barrow.

3. Aircraft observations and operations

The primary observation platform was the NRC Convair-580 (Figure 2), which was instrumented by Environment Canada, NRC, and other ISDAC partners for the in-situ measurements of clouds, aerosols, state parameters, and for the active and passive remote sensing observations listed in Table 3. Measurements of both size-resolved and bulk cloud parameters were made from an unprecedented 20 instruments. The instruments were chosen based on experience obtained during M-PACE and other arctic experiments (e.g., Cober et al. 2001; Lawson et al. 2001). Additional instruments directly measured bulk extinction (Korolev extinctiometer) and condensed mass content (Counterflow Spectrometer and Impactor probe CSI and deep-cone Nevzorov probe). Other instruments recorded particle interarrival times, such as the SPEC fast FSSP. Instruments without shrouds or inlets (e.g., DMT Cloud Droplet Probe, CDP) were added to investigate how large crystal shattering on probe tips might amplify concentrations of particles with maximum dimensions (D) between 1 and 50 μm. Gayet et al. (1996), Field et al. (2003), Korolev and Isaac (2005), McFarquhar et al. (2007b), and Jensen et al. (2009) have suggested such shattering occurs. To quantify uncertainties in size distributions, to ensure no data gaps in the

event a probe malfunctioned, and to test the consistency and performance of multiple probes through closure tests (i.e., extinction and mass derived from size-resolved measurements should match that of probes measuring bulk mass and extinction) redundancy was critical. A two-dimensional stereographic probe (2DS, Lawson et al. 2006), an imaging probe with 10 μm resolution and advanced electronics and optics, was also an important part of the instrument compliment. Its enhancements allow it to detect and image particles with ~ 10 < D < 100 μm that have been difficult in the past to measure with standard two-dimensional cloud (2DC) or Cloud Imaging Probes (CIP).

It was equally important to measure aerosol size, composition, concentration, morphology, optical, and nucleating properties. There were 12 instruments on the NRC Convair-580 for this purpose. A switch was used so that most of the instruments drew from an aerosol inlet in ambient air and from a Counterflow Virtual Impactor (CVI) inlet in cloud, thus permitting characterization of the residual particles upon which the cloud droplets and ice crystals formed. The interior surface of the CVI was gold coated to reduce the influence of crystal impaction on the measured aerosol composition (Murphy et al., 2004). Total number concentrations were measured by a TSI 3775 (D > 4 nm; ambient only) and a TSI 7610 (D > 11 nm; ambient/CVI) condensation particle counters (CPCs), and size distributions were measured for 0.055 < D < 1 μm using an Ultra-High Sensitivity Aerosol Spectrometer (DMT-SPP-200) and for 0.1 < D < 3 μm using a Passive Cavity Aerosol Spectrometer Probe (PMS PCASP-100X). A Continuous Flow Diffusion Chamber (CFDC) measured IN concentration, and a DMT cloud condensation nucleus (CCN) counter measured CCN at two supersaturations. A Time-Resolved Aerosol Collector (TRAC) collected particles with 0.1 < D < 2.5 μm for microscopic analysis (Laskin et al. 2006), and the

first aircraft deployment of the Single particle spectrometer (SPLAT) (Zelenyuk et al., 2009) provided single particle size and composition. All these instruments, except the PCASP, were operated behind the CVI. Aerosol optical properties, critical for knowledge of radiative effects, were measured by a Particle Soot Absorption Photometer (PSAP), a TSI 3563 nephelometer and a new DMT 3-laser photoacoustic and nephelometer (PASS-3) that was deployed on an aircraft for the first time (Flowers et al. 2010). The PASS-3 uses 405, 532, and 781 nm diode lasers aligned in an acoustic resonator to measure light absorption by aerosols at three wavelengths. The PASS-3 also measures simultaneously aerosol total scattering. A combination of these probes allows direct determination of the wavelength dependence (Angstrom exponents) of absorption, scattering and single-scatter albedo (ω_0).

Passive and active remote sensing observations were made by a Ka-band up and down-looking radar and a NAWX (X-band, W-band) dual-polarization Doppler radar, as well as infrared thermometers, broadband radiometers, pyrgeometers and an up-looking G-band passive microwave radiometer. Location and temperature observations were made, together with humidity measurements from a LICOR LIC2GS water vapor/CO_2 instrument, a Buck Research CR-2 chilled mirror, and from an EG&G chilled-mirror hygrometer. Vertical velocities were acquired by a Rosemount 858 gust probe. Although there were some instrumentation failures, the amount of instrument redundancy allowed for almost complete data coverage of important data parameters for the ISDAC period, and sufficient duplication for instrumentation study objectives.

4. Experiment design and execution

Flight plans were developed by a dedicated flight management team using output from numerical weather prediction models, satellite imagery and real-time data

from the NSA site. For a specific day, the plan was designed according to the anticipated cloud and aerosol conditions using an inventory of predetermined plans that had been separately formulated for a) missions or components of missions in the vicinity of Barrow; b) components of flights during transits to and from Barrow; and c) coordinated flights with the NASA B-200 and NOAA P-3 aircraft in the vicinity of Barrow. During the actual mission the on-board flight scientist modified the predetermined plan based on the actual conditions, such as the levels of the cloud and aerosol layers.

The majority of the time the NRC Convair-580 flew in the vicinity of Barrow in order to compare with ground-based remote sensing measurements. Flight profiles consisted of i) spiral profiles over the NSA site, ii) constant altitude legs through cloud, iii) constant altitude legs above or below cloud, iv) missed approaches at the Barrow airport, and v) porpoising maneuvers inside cloud (i.e., ramped ascents and descents). Figure 3 shows the flight track for the second flight on 8 April 2008, when an extensive stratocumulus deck persisted in the vicinity of Barrow all day. The NRC Convair-580 executed all the above profiles except the missed approaches on this day.

On this sortie, the NRC Convair-580 took off from Barrow and immediately ascended through cloud and above, then flying between 1.0 and 1.3 km high on a 180 km leg sampling the aerosol above cloud west northwest of Barrow. Thereafter it descended below cloud to 0.5 km and briefly sampled aerosols from the CVI inlet (i.e., residuals of the precipitation particles). After briefly circling due to air traffic, the NRC Convair-580 flew a constant altitude leg in cloud at 0.8 km, a leg below cloud around 0.5 to 0.6 km sampling from the aerosol inlet, and then another leg in cloud at altitudes between 0.8 and 1.0 km. It then briefly went above cloud to sublimate off ice that had built up on the in-situ probes, and performed a spiral

descent and ascent between 0.5 and 1.0 km over the NSA site. The sortie was completed with a leg measuring aerosols above cloud ascending from 1.0 to 1.2 km, a leg porpoising from cloud top (0.9 to 1.2 km) to base (0.5 km), a leg through cloud (0.7 to 0.8 km) and finally a leg below cloud (0.5 km) to sample residuals of precipitation particles. Similar combinations of legs were flown on other days and allow examinations of how aerosol physical and chemical properties above and below cloud are related to cloud properties.

Due to logistical reasons, the NRC Convair-580 was based out of Fairbanks, Alaska, rather than Barrow. Because 180 minutes were spent flying between Barrow and Fairbanks for each day of flight operations, strategies were implemented to maximize the science return of the experiment. First, at least two sorties were conducted for each flight day, with the NRC Convair-580 landing at Barrow for refueling between sorties. The last sortie involved a return to Fairbanks. On two days (8 and 26 April 2008), the NRC Convair-580 refueled twice at Barrow to maximize the time sampling a single-layer stratocumulus. The transit flights also accomplished additional science goals. The NRC Convair-580 sampled cirrus on six transits (4, 5, 13, 19, 25 and 27 April 2008) to develop an in-situ climatology of the microphysical properties of arctic cirrus, about which little is known. Further, these observations in ice clouds allowed an investigation of whether the shattering of large ice crystals on probe inlets and shrouds artificially amplifies small crystal concentrations. On days when cirrus was not present, additional observations to characterize tropospheric aerosols were made.

5. **Meteorological conditions**

To understand the context of the ISDAC observations, the meteorological and surface conditions are summarized in this section. An important contrast between M-

PACE and ISDAC was that much of the ocean was ice-covered during ISDAC, which could impact cloud properties. Meteorologically, during the first days of April the synoptic pattern was dominated by an upper-level trough in the Aleutians-Bering Strait area. A series of short wave systems propagated around this long wave trough, producing deep precipitating systems over the North Slope as a succession of frontal systems moving through the area.

On 6 April the upper-troposphere jet stream began to shift to a position well south of Alaska. A strong, deep high pressure system developed over the Yukon area, moving slowly northward across the North Pole and into Northern Russia by 14 April. During this period, the upper air synoptic pattern over Alaska was characterized by weak gradients with a high pressure system (1036 – 1044 hPa) dominating the weather for several days. This pushed an arctic air mass across the North Slope with north-easterly to easterly flow with temperatures averaging -21.4 ºC between 8 April and 17 April.

During this time period, a day was encountered on 8 April when a single layer stratocumulus deck formed over the North Slope. The single layer allows the interactions of aerosols and clouds to be more easily isolated without complications of interactions between multiple cloud layers. The extensive low-level deck formed midway between the ridge-line of the north-westward moving high pressure system and a weakening low to its west. The deck existed along the southern and western edge of the upper level ridge, reminiscent of the stratocumulus often observed behind a mid-latitude cold front. This system produced the long-lasting, mixed-phase stratocumulus deck over Barrow. As the synoptic system moved towards the northwest bringing the ridgeline closer to Barrow, the cloud deck gradually thinned.

The weather regime shifted to a distinctly different pattern on 17 and 18 April when a strong upper-level low moved across the North Slope. The surface temperature increased to an average of -8°C with a switch in wind direction from easterly to south-westerly. This system developed into a strong omega block with its ridge line passing south-to-north through central Alaska. This omega block stayed in position for 7 days, producing a succession of deep precipitating systems, each associated with shortwave troughs propagating around the ridge. During this period, a heavily polluted aerosol day occurred on 19 April after the passage of one of the shortwave troughs when the North Slope was in the warm sector behind the front. Some low-level clouds remained over Barrow. Back-trajectories reveal that the air above these low-level clouds originated in central Russia.

The block finally disappeared when a strong low moving eastward from Kamchatka eroded the ridge on 24 April. This low stalled in the Bering Strait where it gradually weakened even while dominating the weather over Barrow. As the low weakened Barrow became more influenced by a high pressure system over the Arctic Ocean, producing another single layered cloud system in weak easterly flow off the ocean on 26 April. Although many other excellent cases with varying degrees of complexity were sampled during ISDAC, preliminary focus has been on these three cases because of their extensive sampling and relatively simple structure.

6. Preliminary Results

Initial work has concentrated on evaluating the quality of the data, and characterizing the properties required for more detailed studies of cloud-aerosol interactions. In this section, some of the observed aerosol and cloud conditions are characterized and results from preliminary scientific investigations summarized.

6.a Ice Nuclei Concentrations

The Texas A&M CFDC measured IN concentrations over a broad range of instrumental operating conditions. While ISDAC was the first field campaign for this specific instrument, comparable IN measurements have been made with similar instruments during SHEBA (Rogers et al. 2001) and M-PACE (Prenni et al. 2009). The CFDC determines in-situ IN concentrations as a function of chosen processing conditions in the CFDC chamber. The IN concentrations were highly variable, ranging from less than 1 L^{-1} to more than 10 L^{-1} with isolated incidents of extremely high concentrations (>100 L^{-1}).

The average concentration of ice-nucleating aerosols in clear air conditions on the ambient inlet at processing temperatures between -10 and -30 ºC for all flights between 8 and 28 April is shown in Figure 4. The data are sorted by water saturation to differentiate between heterogeneous nucleation modes. Data collected below water saturation, that is at supersatuations (SS_w) from -10 to 0%, represent ice crystals formed by deposition freezing whereas data collected above water saturation (0 to 10% SS_w) include all crystals nucleated by immersion, condensation, and depositional freezing. One caveat is that the CFDC is likely to undercount contact freezing nuclei due to limitations in internal mixing and residence time in the chamber. Significant IN concentrations were observed below $SS_w = 0\%$, indicating that depositional nucleation occurred. On all flights when data were collected both above and below $SS_w = 0\%$, the IN concentrations were higher for $SS_w > 0\%$. However, the increase in IN concentration with water saturation was highly variable between days, which suggests that the relative importance of the freezing mechanisms varied. At times, such as during polluted flights on 18 April the airborne particles were highly active as deposition nuclei. On this day, increasing CFDC operational conditions to above

water saturation increased the total IN concentration by only ~6% over the concentrations observed below water saturation.

IN concentrations in the Arctic are generally low, making accurate IN measurements a challenge. Since data collected during times when IN concentrations were below the CFDC detection threshold are not included in the averages in Fig. 4, the averages represent an upper limit to the IN concentrations. For comparison, during periods when the IN counts were below the threshold, the data were reprocessed assuming the IN concentration was zero. These data, representing the lower limit of the measured IN concentrations, are also shown in Fig. 4. Overall, there is a decrease by an average of 36% in the average IN concentrations. In general, both the average IN concentrations and the occasional spikes in IN concentrations observed during ISDAC are similar to previous springtime observations of IN during SHEBA. In contrast, the M-PACE IN concentrations were lower ($\leq$ 1 L^{-1}) and below the CFDC's detection threshold 85% of the time (Verlinde et al., 2007). Collectively, these data suggest a strong seasonal dependence of the aerosol available to act as IN.

6b. Aerosol Composition

SPLAT measures the size and internal composition with 1-sec resolution of individual particles in the 50 nm to 1 μm diameter range as well as particle number concentrations and asphericity factors. The vacuum aerodynamic size distributions were also acquired with between 10 and 60 sec resolution, depending on the number concentrations. During ISDAC, SPLAT measured the size of tens of millions of particles and characterized the internal composition of ~3 million. These data were used to extract the average aerosol density and densities of chemically resolved particle classes that were then used to obtain quantitative information on particle internal compositions. Particles sampled through the aerosol inlet characterize

background aerosol outside of cloud and those sampled through the CVI inlet characterize particles activated as CCN and IN. By comparing the properties of CCN and IN particles to those observed below and above the clouds the types of particles most likely to activate can be quantified.

The SPLAT data indicate a wide range of particle compositions that include sulfates mixed with organics, organic particles composed of various organic compounds, nitrates mixed with organic, processed and freshly emitted sea-salt, dust particles, and biomass burning particles. Many of these particle types appeared in aerosol layers that had horizontal and vertical filamentous structures, in which aerosol number concentration, their size distributions, and compositions varied rapidly along the flight paths. On a number of flights, plumes containing high concentrations of transported biomass burning (BB) particles were encountered. Preliminary analysis of a fraction of the data acquired in ice clouds shows many IN particles were either metallic or composed of dust and that a significant fraction were as small as 100 nm. Of these, perhaps the most interesting observation was an episode on 19 April when copper particles, some as small as 50 nm, served as IN.

A detailed analysis of the single layer stratocumulus cloud sampled on 26 April showed that nearly 90% of the aerosols were activated when this cloud formed. Figure 5 shows the individual particle compositions were varied and included fresh and processed sea salt particles, BB, sulfates mixed with organics, and a large number of organic particles. The comparison between the two pie charts of particles that served as CCN (on left) and of those that were not activated (on right) shows them to be exceptionally similar, indicating that the composition of particles that acted as CCN and those that did not was nearly identical. The SPLAT size distributions in

Figure 6 show that the non-activated particles were appreciably smaller, providing a simple explanation for the difference in CCN activity.

On 19 April 2008 a vast pollution plume lofted from Siberian fires and transported over Alaska (Warnecke et al. 2009) was sampled. Large aerosol absorption indicative of absorbing carbonaceous aerosols and scattering signals were measured by the PASS-3 for a substantial fraction of time during the transit between Fairbanks and Barrow. The aerosol pollution was layered with large enhancements in scattering and absorption at different altitudes. The vertical distribution of ω_0 also showed a vertical structure indicating distinct optical properties for different layers. This information will be used to derive vertical heating rates caused by arctic aerosol pollution that will influence both the dynamics and the clouds.

To understand the chemical origins of changes in observed optical properties the PASS-3 measurements were compared against simultaneous composition measurements made with SPLAT. Fig. 7a shows that, as expected, higher fractions of black carbon corresponded to lower ω_0 at all three wavelengths. Lower ω_0 at 405 nm compared to 532 and 780 nm appears evident where higher concentrations of biomass burning aerosols are present, indicating potential enhanced absorption by coatings and/or organic aerosols at 405 nm (Flowers et al. 2010). In Fig. 7b, for particles that SPLAT indicated were a mixture of soot and sulfate (but not including potentially significant black carbon mass present in biomass burning aerosols seen in Fig. 7a), higher absorption appears to correspond to higher concentrations of black carbon, especially at 532 and 780 nm. The relationship between optical properties is complex and depends strongly on the aerosol mixing state (Jacobsen 2001).

Examples above illustrate a wealth of chemical, microphysical and optical data on aged mixed organic, soot, sulfate, nitrate and salt plumes. The preliminary

results show that the aerosol chemistry and microphysics significantly affect the optical properties. The ISDAC data will be used to test physically-based representations of the relationships between particle size, composition and optical properties developed for climate models and will be especially useful for constraining models of aerosol absorption for arctic conditions.

6c. Investigations of Ice Crystal Shattering

To relate distributions of particle composition and size to the properties of clouds, accurate estimates of cloud microphysical properties are needed. One of the largest uncertainties in characterizing the cloud microphysical properties needed for remote sensing and modelling evaluation studies, as well as fundamental studies of aerosol-cloud interactions, is the uncertain contribution that small ice particles make to the total number concentration, extinction and mass of ice-phase and mixed-phase clouds. Investigations are reducing these uncertainties by comparing concentrations of small particles measured during ISDAC in overlapping size ranges.

Figure 8 shows the number concentration of particles with $3 < D < 50$ μm measured by the FSSP96, $N_{3\text{-}50,FSSP,}$ as a function of that measured by the CDP, hereafter $N_{3\text{-}50,CDP}$, for observations made in cirrus during transits between Fairbanks and Barrow. $N_{3\text{-}50,FSSP}$ is greater by one to two orders of magnitude than $N_{3\text{-}50,CDP}$, and the ratio of $N_{3\text{-}50,FSSP}/N_{3\text{-}50,CDP}$ increases with the concentrations of particles with $D >$ 100 μm measured by the CIP number 2 (CIP2) installed on the CAPS. This discrepancy between $N_{3\text{-}50,FSSP}$ and $N_{3\text{-}50,CDP}$ only existed in ice-phase clouds; there was better agreement in lower-level liquid- and mixed-phase clouds that were typically dominated by water; this suggests shattering of large ice crystals on the FSSP inlet may be causing the discrepancy. McFarquhar et al. (2007b) found similar results for their comparison of concentrations from the CAS and CDP in cirrus during

the Tropical Warm Pool International Cloud Experiment (TWP-ICE). Similarly, concentrations from other FSSPs and the CAS were greater than those from the CDP during ISDAC, with the degree of overestimate depending on the CIP2 concentration.

The 2DS is a newer cloud optical array probe that uses two photodiode arrays attached to fast response electronics to capture two-dimensional images of hydrometeors, with particles as small as 10 μm detected by the probe. This represents a significant improvement over conventional cloud optical array probes, such as the 2DC or CIP. In addition to its higher resolution and better time response for small particles, the 2D-S processing eliminates many shattered particles using an inter-arrival time measurement, as shattered fragments often pass through the probe sample volume in clusters. Thus, a comparison of the concentrations of particles with $10 < D < 50$ μm from the 2DS, hereafter $N_{10\text{-}50,2DS}$, against those derived from the CDP ($N_{10\text{-}50,CDP}$) and FSSP96 ($N_{10\text{-}50,FSSP}$) offers another unique perspective for investigating small crystal measurements. Figure 9 shows no systematic offset between $N_{10\text{-}50,2DS}$ and $N_{10\text{-}50,CDP}$, and no strong dependence of $N_{10\text{-}50,2DS}/N_{10\text{-}50,CDP}$ on the concentration of ice crystals with $D > 100$ μm measured by the CIP2. On the other hand, Figure 10 shows that $N_{10\text{-}50,FSSP}$ is systematically higher than $N_{10\text{-}50,2DS}$. Because the ratio of the number concentration measured by the FSSP to that measured by both the 2DS (shattered particles removed) and CDP is dependent on the large ice crystal concentrations, this suggests measurements of small ice crystals may be affected by the shattering of large ice crystals on inlets and tips.

6d. Examination of Longevity of Mixed-Phase Clouds

Flight profiles executed through single-layer stratocumulus decks on 8 and 26 April 2008 have permitted investigation of factors responsible for the longevity of arctic mixed-phase clouds. Although Figure 11 shows that the mixed-phase clouds

observed on 8 April 2008 appear visually smooth, observations with the NRC X-band radar in Figure 12 show small-scale structure and inhomogeneities in the cloud microphysical characteristics. In particular, Doppler velocities suggest regions of ascent of about 1 m s^{-1} (red color) in close proximity to regions of descent on the order of 1 m s^{-1}. The close coupling of these updrafts and downdrafts is a first indicator of the role of dynamics, mixing and turbulence in these cloud systems (e.g., Shupe et al. 2008).

Figure 13 represents a two-dimensional view of the horizontal and vertical variations in bulk microphysical characteristics derived from probes on the ramped ascents and descents of the NRC Convair-580 during its 180 km long porpoising leg through cloud on 8 April. The blue shading represents the location of the liquid cloud layer identified from the cloud probes. A couple of noteworthy features are evident in Fig. 13: 1) there is a temperature inversion capping the vertical growth of the cloud; 2) the sum of the concentrations derived from the FSSP96 and the PCASP is close to constant throughout and below cloud; 3) there is a gradual increase in LWC with height in the cloud; and 4) although there is a reduction in the concentration and IWC from larger sized ice crystals observed by the 2DP near the cloud top, there is otherwise no large variation with height. Inspection of ice crystals imaged by the in-situ probes indicated that both large and small crystals occurred throughout cloud. The presence of small particles everywhere indicates that either nucleation was occurring throughout cloud or that there was significant vertical mixing. Although the microphysical inhomogeneities and the variability in cloud height for the single-layer stratocumulus sampled on 26 April were not as large (figure not shown), similar trends were noted. McFarquhar et al. (2007a) also noted similar trends in the single layer stratocumulus sampled during M-PACE.

The combination of the inhomogeneities in the radar data (Fig. 12) and the nearly constant ice profiles through cloud (Fig. 13) indicates vertical mixing driven by dynamics or turbulence. Preliminary simulations using the models of Korolev and Isaac (2003) and Korolev and Field (2008) show that harmonic oscillations consistent with the observed velocity fields provide the conditions necessary for the indefinitely long maintenance of these mixed-phase clouds when no precipitation reaches the surface.

6e. Aerosol Effects on Cloud

One science question addressed by ISDAC is the influence of aerosol on cloud microphysical properties. This influence is illustrated in Figure 14, which compares mean number concentrations of cloud droplets and sub-cloud aerosol particles larger than 0.1 μm on six different flights. The droplet and aerosol number concentrations are highly correlated, with some evidence of non-linear dependence, possibly due to suppressed supersaturation at higher aerosol concentrations. This is qualitatively consistent with expectations and has been previously observed (Leaitch et al., 1986; 1996). However, further work is needed to combine these data with updraft velocity and aerosol size and composition data to quantitatively test understanding of aerosol effects on droplet formation. Previous efforts in this area (e.g., Conant et al., 2004, Meskhidze et al., 2005; Fountoukis et al., 2007) did not have bulk composition data, let alone single-particle composition data, to test the dependence of this agreement on composition.

The influence of aerosols on clouds is further illustrated in Figure 15 where the frequency distribution of cloud droplet number concentrations measured by the FSSP96 for flights in single-layer stratocumulus on 8 and 26 April are shown. The concentrations are greater for polluted conditions observed on 26 April than for the

pristine conditions on 8 April, consistent with past studies of liquid-phase clouds (Heymsfield and McFarquhar, 2001). It should also be noted that both the aerosol and droplet concentrations varied by up to a factor of two between the east and west side of the legs flown on 26 April. Future work will explore the dependence of droplet size, ice crystal concentration and ice particle size on aerosol concentration stratifying the extensive ISDAC data according to location in cloud, meteorological forcing and surface conditions.

6f. Surface Spectroradiometer Data

Figure 16 illustrates the usefulness of the surface spectroradiometer data for diagnosing the impact of cloud thermodynamic phase on the radiation budget. In Fig. 17a, downwelling flux spectra obtained 2.5 hours into the first and second flights of 24 April (F-27, F-28) and the flight of 26 April (F-30) are shown. Preliminary analysis of in situ data indicate that the clouds sampled during these flights were composed primarily of ice particles (F-27), a roughly equal mixture of water and ice (F-28), and primarily liquid water (F30). Noticeable contrasts appear in both the spectral dependence and total flux in the 1.6 μm window. The ratio of the flux in the 1.6 μm window to the total broadband flux is plotted in Fig. 17b. At fixed total cloud optical depth and for the solar zenith angle range considered, differences in the flux ratio correspond to differences of 5-10 W m^{-2} between ice-dominated and liquid-dominated cloud microphysics, revealing the influence of cloud phase on surface shortwave radiation.

7. Applications and Modeling

In addition to fundamental studies of cloud and aerosol interactions, there are a number of applications being explored with the data and a number of modelling studies are being conducted. The applications are summarized in Table 4. For each

application, some ISDAC data are used as input to a model, retrieval, or statement of mass balance, and other ISDAC data are used to compare with the output of the model, retrieval, or mass balance. For example, the mass balance application (cloud water closure) provides a consistency test for the bulk and size-resolved measurements and may provide further insight into large ice crystal shattering on probe tips. Some models focus on isolated processes, such as droplet nucleation, while others represent all of the processes that control cloud lifecycle. Retrievals are evaluated so that they can be extended to conditions beyond the period of the ISDAC, which is critically important given the limited time of the ISDAC observations.

ISDAC represents the most comprehensive set of measurements to date for evaluating and improving cloud model and parameterizations, particularly in simulating the mixed-phase cloud regime. ISDAC improves upon past data sets by providing aerosol size/composition data in combination with the wealth of cloud microphysics data that should allow elimination of most shattered artifacts. The longevity of climatically important low level arctic stratus depends critically on cloud microphysics which controls liquid-to-ice conversion and precipitation rates.

Since microphysics process rates are not measured directly, they can be tested via numerical modeling used to obtain a quantitative understanding of these processes. Figure 17 shows one example of such an approach in which a high-resolution cloud model with size-resolved liquid and ice microphysics (Fan et al., 2009) simulated the single-layer stratocumulus sampled on 26 April and demonstrates generally good agreement with observations. The agreement is better within the cloud layer, suggesting that the Bergeron-Findeisen process is reasonably reproduced in the model. Underestimation of below-cloud ice (snow) water content indicate that ice sedimentation rate in the model may be over-predicted.

In addition to cloud-resolving models, a variety of other models of the cloud life cycle are being applied to ISDAC data: single-column, regional, and global models. Simulations with different combinations of ISDAC and M-PACE boundary conditions and aerosol properties are being used to separate the aerosol influence on clouds from the boundary condition influence near Barrow.

8. Summary and Future Work

When combined with the permanent observing facilities at the Department of Energy ground-based facility at Barrow and those specifically installed for ISDAC, the data collected by the NRC Convair-580 constitute the most comprehensive dataset aerosol microphysical and radiative properties and on arctic boundary layer and cirrus microphysical properties ever collected over the North Slope of Alaska. This paper described the science questions that motivated ISDAC and some preliminary science findings. The preliminary analysis presented here has also shown the importance of considering dynamical, mixing and turbulent processes when examining aerosol indirect and semi-direct effects on clouds. Most ISDAC data are available from the ARM data archive at http://www.archive.arm.gov/, and hence are open to additional investigations from the scientific community.

During the next few years the ISDAC data will be used to (a) test current understanding of droplet and crystal nucleation, (b) improve understanding of aerosol effects on the lifecycle and radiative properties of mixed-phase clouds, (c) evaluate and improve the representation of cloud processes in a variety of cloud models, and (d) test and improve remote sensing retrievals of cloud and aerosol properties from the surface and from space. Both the spiral profiles over the NSA site and some CloudSat/CALIPSO validation flights are available for the later purpose. The results for the ISDAC period, when aerosol concentrations were relatively high, will be

contrasted with those for the more pristine M-PACE period, to assess the ability of cloud models to simulate the differences. These evaluations will guide improvements in the cloud models for the purpose of improving simulations of clouds and aerosols across the arctic basin. Ultimately these improvements will be used to explain the role of clouds and aerosols in the loss of arctic sea ice and improve reliability of projections of future changes in arctic climate.

Acknowledgements: ISDAC was supported by the United States Department of Energy (DOE) Atmospheric Radiation Measurement (ARM) Program Climate Research Facility, the DOE Atmospheric Sciences Program, the National Research Council of Canada and Environment Canada. We are indebted to the many scientists and staff who participated in the ISDAC field project, without whose efforts this work would have been possible. Data were obtained from the ARM program archive, sponsored by DOE, Office of Science, Office of Biological and Environmental Research (BER) Environmental Science Division. This work was sponsored by grants DE-FG02-02ER63337, DE-FG02-07ER64378, DE-FG02-06ER64167, and DE-FG02-09ER64770 as part of ARM. The Pacific Northwest National Laboratory is operated for DOE by Battelle Memorial Institute under contract DE-AC06-76RLO1830. LANL acknowledge the ongoing support from ASP for the acquisition and development of the PASS-3. Prepared in part by LLNL under Contract DE-AC52-07NA27344.

References

ACIA, Arctic Climate Impact Assessment - Scientific Report, 1046 (Cambridge Univ. Press), 2005.

Albrecht, B.A., 1989: Aerosols, cloud microphysics, and fractional cloudiness, *Science*, **245**, 1227-1230.

Barrie, L. A., 1986: Arctic air pollution: An overview of current knowledge. *Atmos. Environ*., 20, 643– 663.

Boe, J., A. Hall, X. Qu, 2009: September sea-ice cover in the Arctic projected to vanish 2100. *Nature Geoscience*, doi.10.1038/ngeo467.

Cober, S. G., G. A. Isaac, A. V. Korolev, and J. W. Strapp, 2001: Assessing cloud-phase conditions. *J. Appl. Meteor., 40,* 1967-1983.

Conant, W.C., and Coauthors, 2004: Aerosol–cloud drop concentration closure in warm cumulus, *J. Geophys. Res*., *109*, D13204, doi:10.1029/2003JD004324.

Curry, J.A., J. Schramm, and E.E. Ebert, 1993: Impact of clouds on the surface radiation budget of the Arctic Ocean. *Meteor. and Atmos. Phys*., 57, 197-217.

Curry, J. A., and Coauthors, 2000: FIRE Arctic Clouds Experiment. *Bull. Amer. Meteor. Soc*., 81, 5–30.

Dong, X., G. G. Mace, P. Minnis, and D. F. Young, 2001: Arctic stratus cloud properties and their effect on the surface radiation budget: Selected cases from FIRE ACE, *J. Geophys. Res., 106*, 15297-15312.

Fan, J., M. Ovtchinnikov, J. M. Comstock, S. A. McFarlane, and A. Khain, 2009: Ice formation in Arctic mixed-phase clouds: Insights from a 3-D cloud-resolving model with size-resolved aerosol and cloud microphysics, *J. Geophys. Res*., *114*, D04205, doi:10.1029/2008JD010782.

Field, P.R., R. Wood, P. R. A. Brown, P. H. Kaye, E. Hirst, R. Greenaway, and J. A. Smith, 2003: Ice Particle Interarrival Times Measured with a Fast FSSP. *J. Atmos. Ocean. Tech. 20,* 249–261.

Flowers, B., M.K. Dubey, E.A. Stone, J.J. Schauer, C. Mazzoleni and S. Kim, 2010: Optical properties of mixed carbonaceous aerosols observed at Jeju South Korea with a 3-laser photoacoustic spectrometer: Correlation with chemical composition. *Geophys. Res. Lett.*, Under review.

Fountoukis, C., and Coauthors, 2007: Aerosol-cloud drop concentration closure for clouds sampled during ICARTT, *J. Geophys. Res*., *112*, D10S30, doi:10.1029/2006JD007272.

Fridlind, A. M., A. S. Ackerman, G. McFarquhar, G. Zhang, M. R. Poellot, P. J. DeMott, A. J. Prenni, and A. J. Heymsfield, 2007: Ice properties of single-layer stratocumulus during the Mixed-Phase Arctic Cloud Experiment (M-PACE): Part II, Model results. *J. Geophys. Res., 112*, D24202, doi:10.1029/2007JD008646.

Garrett T.J., and C. Zhao, 2006: Increased Arctic cloud long wave emissivity associated with pollution from mid-latitudes, *Nature*, 440, 787-789.

Gayet, J. G., G. Febvre, and H. Larsen, 1996: The reliability of the PMS FSSP in the presence of small ice crystals. *J. Atmos. Oceanic Technol., 13,* 1300–1310.

Hansen, A.D.A., T.J. Conway, L.P. Strele, B.A. Bodhaine, K.W. Thoning, P. Tans and T. Novakov, 1989: Correlations among combustion effluent species at Barrow, Alaska: Aerosol black carbon, carbon dioxide, and methane. *J. Atmos. Chem.*, 9, 283 – 299.

Hansen, J.E., M. Sato, and R. Ruedy, 1997b: Radiative forcing and climate response, *J. Geophys. Res*., 102, 6831–6864.

Hara, K., S. Yamagata, T. Yamanouchi, K. Sato, A. Herber, Y. Iwasaka, M. Nagatani, and H. Nakata, 2003: Mixing states of individual aerosol particles in spring Arctic troposphere during ASTAR 2000 campaign, *J. Geophys. Res.*, 108(D7), AAC2-1-12.

Harrington, J.Y., and P.Q. Olsson, 2001: On the potential influence of ice nuclei on surface-forced marine stratocumulus cloud dynamics, *J. Geophys. Res.,* 106, 27473-27484.

Harrington, J.Y., T. Reisin, W.R. Cotton and S.M. Kreidenweis, 1999: Cloud resolving simulations of Arctic stratus. Part II: Transition-season clouds, *Atmos. Res., 51*, 45-75.

Heymsfield, A.J., and G.M. McFarquhar, 2001: Microphysics of INDOEX clean and polluted trade cumulus clouds. *J. Geophys. Res*., **106**, 28653-28673.

Hobbs, P.V., and A.L. Rangno, 1998: Microstructures of low and middle-level clouds over the Beaufort Sea, *Quart. J. Roy. Meteor. Soc., 124,* 2035-2071.

Inoue, J., J. Liu, J.O. Pinto and J.A. Curry, 2006: Intercomparison of arctic regional climate models: Modeling clouds and radiation for SHEBA in May 1998. *J. Climate*, **19**, 4167-4178.

Intrieri, J.M., M.D. Shupe, T. Uttal and B.J. McCarty (2002a), An annual cycle of Arctic cloud characteristics observed by radar and lidar at SHEBA, *J. Geophys. Res., 107,* 10.1029/2000JC000423.

IPCC, 2007: *Climate Change 2007: The Physical Science Basis. Contribution of Working Group I to the Fourth Assessment Report of the Intergovernmental Panel on Climate Change* [Solomon, S., D. Qin, M. Manning (eds.)].

Jacob, D.J**.,** J.H. Crawford, H. Maring, A.D. Clarke, J.E. Dibb, R.A. Ferrare, C.A. Hostetler, P.B. Russell, H.B. Singh, A.M. Thompson, G.E. Shaw, E.

McCauley, J.R. Pederson, and J.A. Fisher, 2009: The ARCTAS aircraft mission: design and execution *, Atmos. Chem. Phys. Discuss.*, **9**, 17073-17123.

Jacobson, M.Z., 2001: Strong radiative heating due to the mixing state of black carbon. *Nature*, **409**, 695-697.

Jensen, E.J., and Coauthors, 2009: On the importance of small ice crystals in tropical anvil cirrus. *Atmos. Chem. Phys.*, **9**, 5519-5537.

Kay, J. E., and A. Gettelman, 2009: Cloud influence on and response to seasonal Arctic sea ice loss, *J. Geophys. Res.*, *114*, D18204, doi:10.1029/2009JD011773.

Klein, S.A., and Coauthors, 2008: Intercomparison of model simulations of mixed-phase clouds observed during the ARM Mixed-Phase Arctic Cloud Experiment. Part I: Single layer cloud. *Quart. J. Roy. Meteor. Soc.*, **135**, 979-1002.

Korolev, A.V., and G.A. Isaac, 2003: Phase transformation of mixed-phase clouds. *Quart. J. Roy. Meteor. Soc.*, **129**, 19-38.

Korolev A. V., and G. A. Isaac, 2005: Shattering during sampling by OAPs and HVPS. Part I: Snow particles, *J. Atmos. Oceanic Technol., 22*, 528–543.

Korolev, A.V., and P.R. Field, 2008: The effect of dynamics on mixed-phase clouds: theoretical considerations. *J. Atmos. Sci.*, **65**, 66-86.

Laskin, A., J.P. Cowin, M.J. Iedema, 2006: Analysis of individual environmental particles using modern methods of electron microscopy and X-ray microanalysis. *J. Electron Spectroscopy and Related Phenomena*, **150**, 260-274.

Lawson, R., B.A. Baker, C.G. Schmitt, and T.L. Jensen, 2001: An overview of microphysical properties of Arctic clouds observed in May and July 1998 during FIRE ACE, *J. Geophys. Res.*, 106, 14989-15014.

Lawson R. P., D. O'Connor, P. Zmarzly, K. Weaver, B. A. Baker, Q. Mo, and H. Jonsson, 2006: The 2D-S (stereo) probe: Design and preliminary tests of a new airborne, high-speed, high-resolution particle imaging probe, *J. Atmos. Oceanic Technol., 23,* 1462–1477.

Leaitch, W.R., Strapp, J.W., Isaac, G.A., and Hudson, J.G., 1986: Cloud droplet nucleation and cloud scavenging of aerosol sulphate in polluted atmospheres. Tellus, **38B**, 328-344.

Leaitch, W., C. Banic, G. Isaac, M. Couture, P. Liu, I. Gultepe, S.-M. Li, L. Kleinman, P. Daum, and J. MacPherson, 1996: Physical and chemical observations in marine stratus during the 1993 North Atlantic Regional Experiment: Factors controlling cloud droplet number concentrations, J. Geophys. Res., 101(D22), 29123-29135.

Lubin, D. and A.M. Vogelmann, 2006: A climatologically significant aerosol longwave indirect effect in the Arctic. *Nature*, 439, 453-456.

McConnell, J. R., R. Edwards, G.L. Kok, M.G. Flanner, C.S. Zender, E.S. Saltzman, J.R. Banta, D.R. Pasteris, M.M. Carter, and J.D.L. Kahl, 2007: 20th-Century Industrial black carbon emissions altered Arctic climate forcing, *Science*, **317**, 1381–1384.

McFarquhar, G.M., G. Zhang, M.R. Poellot, G.L. Kok, R. McCoy, T. Tooman, and A.J. Heymsfield, 2007a: Ice properties of single layer stratocumulus during the Mixed-Phase Arctic Cloud Experiment (MPACE). Part I: Observations. *J. Geophys. Res.*, **112**, D24202, doi:10.1029/2007JD008646.

McFarquhar, G.M., J. Um, M. Freer, D. Baumgardner, G.L. Kok and G. Mace, 2007b: The importance of small ice crystals to cirrus properties: Observations from the Tropical Western Pacific International Cloud Experiment (TWP-ICE). *Geophys. Res. Lett.*, *34,* L13803, doi:10.1029/2007GL029865.

Meskhidze, N., A. Nenes, W. C. Conant, and J. H. Seinfeld (2005), Evaluation of a new cloud droplet activation parameterization with in situ data from CRYSTAL-FACE and CSTRIPE, *J. Geophys. Res*., *110*, D16202, doi:10.1029/2004JD005703.

Min, Q. and L.C. Harrison, 1996: Cloud properties derived from surface MFRSR measurements and comparison with GOES results at the ARM SGP site. *Geophys. Res. Lett*., **23**, 1641-1644.

Morrison H., J. O. Pinto, J. A. Curry, and M. McFarquhar, 2008: Sensitivity of modeled arctic mixed-phase stratocumulus to cloud condensation and ice nuclei over regionally-varying surface conditions, *J. Geophys. Res*., 113, D05203, doi:10.1029/2007JD008729.

Morrison, H., and 27 Co-authors, 2009: Intercomparison of model simulations of mixed-phase clouds observed during the ARM Mixed-Phase Arctic Cloud Experiment, Part II: Multi-layered cloud, *Quart. J. Roy. Meteorol. Soc*., **135**, 1003-1019.

Murphy, D. M., Cziczo, D. J., Hudson, P. K., Thomson, D. S., Wilson, J. C., Kojima, T., and Buseck, P. R., 2004: Particle generation and resuspension in aircraft inlets when flying in clouds, *Aerosol Sci. Technol*., *38*, 400–408.

Pincus, R., and M. B. Baker, 1994: Effect of precipitation on the albedo susceptibility of clouds in the marine boundary layer. *Nature*, **372**, 250-252.

Pinto, J.O., 1998: Autumnal mixed-phased cloudy boundary layers in the Arctic, *J. Atmos. Sci., 55,* 2016-2038.

Prenni, A.J., P.J. DeMott, D.C. Rogers, S.M. Kreidenweis, G.M. McFarquhar, G. Zhang and M.R. Poellot: Ice nuclei characteristics from M-PACE and their relation to ice formation in clouds, *Tellus B*, 2009 (In press).

Quinn, P.K., T.L. Miller, T.S. Bates, J.A. Ogren, E. Andrews, and G.E. Shaw, 2002: A 3-year record of simultaneously measured aerosol chemical and optical properties at Barrow, Alaska. *J. Geophys. Res.*, 107(D11), doi:10.1029/2001JD001248.

Quinn, P. K., T. S. Bates, E. Baum, N. Doubleday, A. M. Fiore, M. Flanner, A. Fridlind, T. J. Garrett, D. Koch, S. Menon, D. Shindell, A. Stohl, and S. G. Warren, 2008: Short-lived pollutants in the Arctic: their climate impact and possible mitigation strategies. *Atmos. Chem. Phys*., 8, 1723–1735.

Rogers, D.C., P.J. DeMott and S.M. Kreidenweis, 2001: Airborne measurements of tropospheric ice-nucleating aerosol particles in the Arctic spring, *J. Geophys. Res*., 106, 15,053-15,063.

Sednev, I., S. Menon, G. McFarquhar, and A.D. Del Genio, 2008: Simulating mixed-phase Arctic stratus clouds: sensitivity to ice initiation mechanisms. *Atmos. Chem. Phys.*, **8**, 11755-11819.

Shaw, G.E. Atmospheric turbidity in the polar regions. *J. Appl. Meteorol*., *21*, 1080-1088, 1982.

Sherwood, S., Aerosols and ice particle size in tropical cumulonimbus. *J. Climate*, *15*, No. 9, 2002, pp 1051-1063, 2002.

Shindell, D., and G. Faluvegi, 2009: Climate response to regional radiative forcing during the twentieth century, *Nature Geosci.*, *2*, 294-300, DOI: 10.1038/NGEO473.

Shupe, M.D,. and J.M. Intrieri, 2004: Cloud radiative forcing of the Arctic surface: The influence of cloud properties, surface albedo and solar zenith angle. *J. Climate*, **17**, 616-628.

Shupe, M.D., T. Uttal, and S.Y. Matrosov, 2005: Arctic cloud microphysics retrievals from surface-based remote sensors at SHEBA, *J. Appl. Meteor.,* 44**,** 1544–1562.

Shupe, M. D., S.Y.Y. Matrosov, and T. Uttal, 2006: Arctic mixed-phase cloud properties derived from surface-based sensors at SHEBA. *J. Atmos. Sci*., 63, 697-811.

Shupe, M. D., P. Kollias, P. O. G. Persson, and G. M. McFarquhar, 2008: Vertical motions in Arctic stratiform mixed-phase clouds. *J. Atmos. Sci*., **65**, 1304-1322.

Stroeve, J., M.K. Holland, W. Meier, T. Scambos, M. Serreze, 2007: Arctic sea ice decline: faster than forecast. *Geophys. Res. Lett.*, 34, L09501, doi:10.1029/2007GL029703.

Sun, Z., and K.P. Shine, 1994: Studies of the radiative properties of ice and mixed-phase clouds. *Quart. J. Roy. Meteor. Soc.*, **120**, 111-137.

Turner, D.D., 2005: Arctic mixed-phase cloud properties from AERI-lidar observations: Algorithm and results from SHEBA. *J. Appl. Meteor.*, **21**, 1790-1808.

Turner, D.D., S.A. Clough, J.C. Liljegren, E.E. Clothiaux, K. Cady-Pereira, and K.L. Gaustad, 2007: Retrieving liquid water path and precipitable water vapor from

Atmospheric Radiation Measurement (ARM) microwave radiometers. *IEEE Trans. Geosci. Remote Sens.*, **45**, 3680-3690, doi:10.1109/TGRS.2007.903703.

Twomey, S., 1974: Pollution and the planetary albedo. *Atmos. Environ.*, **8**, 1251-1256.

Uttal, T., and Co-authors, 2002: The Surface Heat Budget of the Arctic Ocean, *Bull. Amer. Meteor. Soc*., 83, 255-275.

Vavrus, S., 2004: The impact of cloud feedbacks on Arctic climate under greenhouse forcing, *J. Climate, 17*, 603–615.

Verlinde, J., and Co-authors, 2007: The mixed-phase Arctic cloud experiment, *Bull. Am. Meteorol. Soc., 88*, 205-221.

Walsh, J.E., and W.L. Chapman, 1998: Arctic cloud-radiation-temperature associations in observational data and atmospheric reanalyses*, J. Climate, 11*, 3030-3045.

Wang, M., and J.E. Overland, 2009: A sea ice free summer Arctic within 30 years?, *Gephys. Res. Lett.*, 36, L07502, doi:10.102009GL037820.

Warneke, C., and Co-authors, 2009: Biomass burning in Siberia and Kazakhstan as an important source for haze over the Alaskan Arctic in April 2008, *Geophys. Res. Lett.*, 36, L02813, doi:10.1029/2008GL036194.

Yum, S.S., and J. G. Hudson, 2001: Vertical distributions of cloud condensation nuclei spectra over the Springtime Arctic Ocean. *J. Geophys. Res.*, **106**, 15045-15052.

Zelenyuk A, Yang J, Imre D, & Choi E (2009) SPLAT II: An aircraft compatible, ultra-sensitive, high precision instrument for in-situ characterization of the

size and composition of fine and ultrafine particles. *Aerosol Science and Technology* 43:411-424.

Tables Captions

Table 1: The primary science questions addressed during ISDAC.

Table 2: Instruments and measurements at ARM Barrow site during ISDAC experiment.

Table 3: Instruments installed on the NRC Convair-580 during ISDAC. Although most probes installed on each flight, a few probes were exchanged and only used for specific flights (e.g., two-dimensional probes with new tips designed to reduce shattering, the SPEC fast FSSP, and the CIP1.

Table 4: List of applications being explored with the ISDAC data.

Figure Captions

Figure 1: Photograph of the Barrow NSA Site with additional instruments installed for ISDAC labelled and noted in the caption (Photo credit: I. Gultepe).

Figure 2: Photo of NRC Convair-580 taking off from Fairbanks during ISDAC. Multiple probes can be seen hanging from wings (Photo credit: ?)

Figure 3: Flight track flown by NRC Convair-580 on Sortie #16, 8 April 2008. Constant altitude flight legs flown above, below and within cloud, together with ramped ascents and descents through cloud and spirals over NSA site depicted. Red represents locations where clouds were sampled, with cloud identified as locations where 10-s averaged CSI total water content > 0.001 g m^{-3}.

Figure 4: Average IN concentrations measured below (-10 to 0% SS_w) and above water saturation (0 to +10% SS_w) shown as solid diamonds and triangles, respectively, as function of flight number. In addition, lower limits to the IN concentrations below (-10 to 0% SS_w) and above water saturation (0 to +10% SS_w) are shown as open diamonds and triangles, respectively. Data in the figure were collected by sampling on the ambient inlet during clear air conditions.

Figure 5: Pie charts showing the compositions of particles that were activated to form cloud droplets (left) and the composition of particles, in the very same air-mass, that were not activated. Observations acquired on 26 April.

Figure 6: The SPLAT measured size distribution of the particles that activated to form cloud droplets (blue) and of particles that were not activated (black). Observations acquired on 26 April.

Figure 7: a) Measured ω_0 (780, 532, 405nm) for selected periods on 19 April 2008. Chemical composition of aerosol derived from SPLAT also shown. b) Absorption (left axis) at 3 wavelengths and black carbon mass concentration measured by SPLAT

over same time periods contained in particles that are a mixture of soot and sulfate only; this does not include black carbon mass present in biomass burning aerosols seen in pie charts in a.

Figure 8: $N_{3\text{-}50,FSSP}$ as function of $N_{3\text{-}50,CDP}$ for measurements made in cirrus during transits between Fairbanks and Barrow on 4, 5, 13, 19 and 25 April 2008. Different dates are indicated by different symbols. Colors indicate different concentration of particles with D > 100 μm measured by the CIP2.

Figure 9: $N_{3\text{-}50,2DS}$ as function of $N_{3\text{-}50,CDP}$ for measurements made in cirrus during transits between Fairbanks and Barrow on 4, 5, 13, 19 and 25 April 2008. Different dates are indicated by different symbols. Colors indicate different concentration of particles with D > 100 μm measured by the CIP2.

Figure 10: $N_{3\text{-}50,2DS}$ as function of $N_{3\text{-}50,FSSP}$ for measurements made in cirrus during transits between Fairbanks and Barrow on 4, 5, 13, 19 and 25 April 2008. Different dates are indicated by different symbols. Colors indicate different concentration of particles with D > 100 μm measured by the CIP2.

Figure 11: Image of single-layer stratocumulus deck sampled by NRC Convair-580 on 8 April 2008. Glory and shadow of aircraft are seen in photo. Photo taken by Alexei Korolev when NRC Convair-580 was executing flight leg above deck.

Figure 12: Cross-section of Doppler velocity (V), with negative values indicating upward motion, and reflectivity (Z) measured by NRC X-band radar during constant altitude leg flight above single-layer stratocumulus deck on 8 April 2008.

Figure 13: Vertical profile of a) temperature, b) cloud droplet number concentration from FSSP96 (N_d) and aerosol concentration from PCASP (N_a), c) $N_d + N_a$, d) liquid water content derived from FSSP96 size distribution and directly measured by Nevzorov probe, e) ice water content derived from size distribution measured by 2DP,

and f) ice crystal concentration derived from 2DP. Each vertical profile was obtained during a single ramped ascent or descent during the leg when NRC Convair-580 porpoised from cloud top to bottom during Sortie 16 on 8 April 2008. Blue shading, based on analysis of individual profiles, represents location of liquid cloud layer on each profile.

Figure 14: Mean concentrations of cloud droplets and sub-cloud aerosol particles larger than 0.1 μm on 6 different flights during ISDAC.

Figure 15: Frequency distribution of number concentration measured by FSSP96 in liquid and mixed-phase clouds for single-layer stratocumulus sampled on 8 and 26 April 2008. Each measurement represents a 1-s average or approximately 120 m of track length.

Figure 16. (A) Downwelling surface spectral flux obtained from the ASD (Inc.) spectroradiometer at NSA under flights F-27 and F-28 on 24 April and under flight F-30 on 26 April (F-30), 2008. The spectra were obtained approximately 2.5 hours into each flight. (B) For the duration of these three flights, the ratio of the surface flux in the 1.6 μm window to the broadband flux, in five minute intervals.

Figure 17: Model predicted (lines) and observed (diamonds) mean vertical profiles of mixed-phase cloud parameters (liquid, Ql, and ice, Qi, mass mixing ratios, droplet, Nd, and ice particle, Ni, number mixing ratios and liquid water condensate fraction) for Sortie # 31 on 26 April 2008. Shaded area and horizontal lines indicate 15 to 85 percentile ranges for simulated and measured parameters, respectively.

Tables

How do properties of the arctic aerosol during April differ from those measured during the Mixed-Phase Arctic Cloud Experiment (M-PACE) in October?
To what extent do different properties of the arctic aerosol during April produce differences in the microphysical and macrophysical properties of clouds and the surface energy balance?
To what extent can cloud models and the cloud parameterizations used in climate models simulate the sensitivity of arctic clouds and the surface energy budget to the differences in aerosol between April and October?
How well can long-term surface-based measurements at the ARM Climate Research Facility (ACRF) North Slope of Alaska (NSA) locale provide retrievals of aerosol, cloud, precipitation, and radiative heating in the Arctic?

Table 1: The primary science questions addressed during ISDAC.

Instrument	Measurements/Derived Quantities
Radiosonde	Profiles of temperature, humidity and winds
Microwave radiometer	Water vapor path, liquid water path
Microwave radiometer profiler	Temperature, humidity
915 MHz radar wind profiler/RASS	Winds, virtual temperature profile
Vaisala Ceilometer	Cloud base altitude
Millimeter cloud radar	Cloud liquid water, cloud ice content profiles
Micropulse lidar (polarized)	Backscatter profile, depolarization ratio
Atmospheric Emitted Radiance Interferometer (AERI)	Downwelling high-resolution infrared radiance spectra, profile of temperature and humidity, water path, optical depth, cloud thermodynamic phase, and effective radius of ice and water
Cimel sunphotometer	Aerosol optical depth
Multi-Filter Shadowband Radiometer	Aerosol optical depth at multiple wavelengths
Normal incidence multifilter radiometer	Aerosol optical depth
Upviewing radiometers	Downwelling longwave and shortwave radiance
Downviewing radiometers	Upwelling longwave, shortwave radiance
Hotplate (TPS) precipitation sensor	Precipitation
Disdrometer	Precipitation rate, extinction
Humidified nephelometer	Aerosol scattering as function of relative humidity
PSAP	Aerosol absorption
Condensation nuclei counter	Total particle number
PCASP	Accumulation mode size distribution
CCN	CCN concentration (one supersatation at a time)
Daily chemical analysis	Submicron mass, ion concentration

Ice particle counter (IPC)	Ice particle concentration
DMIST Visibility sensor/camera	Visibility
FD1sP precipitation and visibility sensor	Precipitation and visibility
VRG101 precipitation instrument	Precipitation
FMD droplet spectra	Cloud droplet size distributions
Vaisala surface temperature sensor	Temperature
Vaisala water phase sensor	Water phase
Turbulence measurements	Turbulence
Snow gauge	Snow depth
ASD Spectroradiometer	Shortwave spectral irradiance
Tandem Differential Mobility Analyzer	Aerosol composition

Table 2: Instruments and measurements at ARM Barrow site during ISDAC experiment.

Instrument	Measurements and/or Derived Quantities
Rosemont 102 probes (3)	Temperature
NCAR Reverse flow probe	Temperature
NRC position measurement system	Aircraft positions, attitudes, etc
NRC wind measurement system	Winds and gusts
EG&G chilled mirror hygrometer	Humidity
LICOR LIC2G2 water vapor/CO2 instrument	Humidity
Buck Research CR-2 chilled mirror hygrometer	Humidity
Rosemount 858 gust probe	Vertical velocity
Rosemount Icing Probe (RICE)	Presence of supercooled water
Nevzorov LWC/TWC Probe	Liquid water content & total water content
PMS CSIRO King Probe	Liquid water content
Vibrameter	Total water content
DMT Cloud Spectrometer and Impactor (CSI)	Total condensed water content from counter-flow evaporator, and droplet size distributions from attached CDP (see separate item below)
DMT Cloud Droplet Probe (CDP)	Cloud size distributions (2 to 50 μm) attached to CSI above
Korolev cloud extinction meter	Cloud extinction
DMT Cloud, Aerosol and Precipitation Spectrometer (CAPS)	Cloud size distributions: Cloud and Aerosol Spectrometer CAS (1 to 50 μm), Cloud Imaging Probe CIP2 (25 to 1550 μm)
DMT CIP1	Cloud size distributions (15 to 960 μm)
SPEC Cloud Particle Imager (CPI)	2.3 μm resolution images of cloud particles
SPEC 2D-S Cloud Spectrometer	Cloud size distributions and images (10 to 1280 μm); 2

	independent orthogonal views of particle population
PMS Forward Scattering Spectrometer Probe (FSSP)-100 X (96)	Cloud size distributions (2 to 47 μm)
PMS FSSP-100X (124)	Cloud size distributions (2 to 47 μm)
PMS FSSP-300	Cloud size distributions (0.3 to 20 μm)
PMS Two Dimensional Cloud Probe (2DC)	Cloud size distributions and cloud images (25 to 800 μm)
PMS Two Dimensional Precipitation Probe (2DP)	Precipitation size distributions and precipitation images (200 to 6400 μm)
PMS 2DC Grey	Grey-scale images of cloud particles, 15-960 μm
TSI 3775	Total aerosol concentration (D > 4 nm)
TSI 7610	Total aerosol concentration (D > 11 nm)
PMS Passive Cavity Aerosol Spectrometer Probe (PCASP-100X)	Aerosol size distribution (~100 to 3000 nm)
DMT Cloud Condensation Nuclei (CCN) Counter	CCN concentration
Continuous Flow Diffusion Chamber (CFDC)	Ice nuclei (IN) concentration
Radiance Particle/Soot Absorption Photometer (PSAP)	Mass of black carbon in air
DMT 3-laser photoacoustic and nephelometer (PASS-3)	Light absorption of aerosols at 3 wavelengths
TSI 3563 Nephelometer	Optical scattering properties
Single Particle Laser Ablation Time of flight mass spectrometer (SPLAT)	Single particle size-resolved composition of refractory and non-refractory material

Time-Resolved Aerosol Collector (TRAC), 2 samplers	Sampling of airborne particles for spectro-microscopy laboratory analysis, 0.1 to 2.5 μm
Counterflow Virtual Impactor	Separation of residual aerosol
DMT Ultra-high sensitivity aerosol spectrometer	Aerosol size distribution 55 to 1000 nm
Tecran continuous Hg analyzer (ARQD)	Mercury
TECO Model 49 Ozone analyzer	Ozone
Modified Teco Model 48 CO analyzer	Carbon monoxide
Heitronics KT19.85 Infrared Thermometer	Nadir narrow-field IR temperature below aircraft
Broadband visible radiometers	Broadband hemispheric visible radiation, zenith and nadir view, 305-2800 nm
Broadband pyrgeometer (Epply 3.5 to 50 μm)	Broadband hemispheric infrared fluxes, zenith and nadir view
ProSensing Up-looking G-band radiometer	Multichannel radiometer centered on 183.31 GHz measuring downwelling microwave radiance
Ka-band up and down-looking radar	Cross-sections of radar reflectivity
NAWX X-band/W-band radar, dual polarization, dopplerized, up/down/side looking	Cross-sections of radar reflectivity and size-looking reflectivity/Doppler velocity fields

Table 3: Instruments installed on the NRC Convair-580 during ISDAC. Although most probes installed on each flight, a few probes were exchanged and only used for

specific flights (e.g., two-dimensional probes with new tips designed to reduce shattering, the SPEC fast FSSP, and the CIP1.

Application	Input Data	Instrument	Validation data	Instrument
CCN closure	Aerosol size distributions	PCASP	CCN concentration	DMT CCN
Droplet number closure	Aerosol size distributions and vertical velocities	PCASP, gust probes	Droplet number concentration	CDP, CAS, FSSPs
Cloud extinction closure	Cloud particle size distributions	CDP, CAS, FSSPs, 2DC, CIP, 2DP	Cloud extinction	Extinctiometer
Cloud water closure	Cloud particle size distributions	CDP, CAS, FSSPs, 2DC, CIPs, 2DP	Total water content (TWC)	CSI, Nevzorov probe
Cloud modeling	Aerosol size distributions, ice nuclei concentrations, radiative fluxes at model top, profiles of horizontal and vertical velocities, temperature and moisture, and surface fluxes and large-scale forcing	PCASP, CFDC, pyrgeometers, ECMWF reanalysis	Cloud particle size distributions, liquid water and total water content, precipitation and cloud extinction	CDP, CAS, FSSPs, 2DC, CIPs, 2DP, LWC probes, Nevzorov probe, CSI, Extinction meter, Hot-plate rain gauge, etc.
Semi-direct effect	Same as for cloud modeling, plus aerosol absorption and scattering	Same as for cloud modeling, plus PSAP and nepheometer	Same as for cloud modeling	Same as for cloud modeling
Relation between IN and aerosol composition	Ice crystal concentration	CFDC	Size-resolved aerosol composition	Single particle mass spectrometer
Relation	Ice crystal concentration,	CFDC	Crystal size and habit and	CPI, CDP, CAS,

between IN and ice crystal concentration	temperature and humidity		cloud particle size distributions	FSSPs, 2DC, CIPs, 2DP
Aerosol extinction retrieval	Aerosol extinction	MPL	Aerosol scattering and absorption	Nephelometer and PSAP
CCN retrieval	Aerosol backscatter and scattering, relative humidity retrieval, surface CCN and humidification function	MPL, RASS, Surface CCN and nephelometer	Cloud condensation nuclei concentration	DMT CCN
MMCR retrievals	Derived profiles of liquid water and ice water content	MMCR	Liquid water and total water content	LWC probes, Nevzorov probe & CSI
MWR retrievals	Derived liquid water path and retrieval of liquid water content	MWR	Liquid water content	King probe Nevzorov
AERI retrievals	Derived droplet and crystal optical depth, liquid and ice water path, droplet and crystal effective radius	AERI	Liquid water and total water content, cloud particle size distributions, cloud extinction	LWC probes, Nevzorov, CSI, CAS, CDP, FSSPs, CIPs, 2DC, 2DP, Extinction meter
ASD retrievals	Cloud optical depth, cloud water path, effective radius	ASD spectro-radiometer	Same as for AERI	Same as for AERI

Table 4: List of applications being explored with the ISDAC data

Figure captions

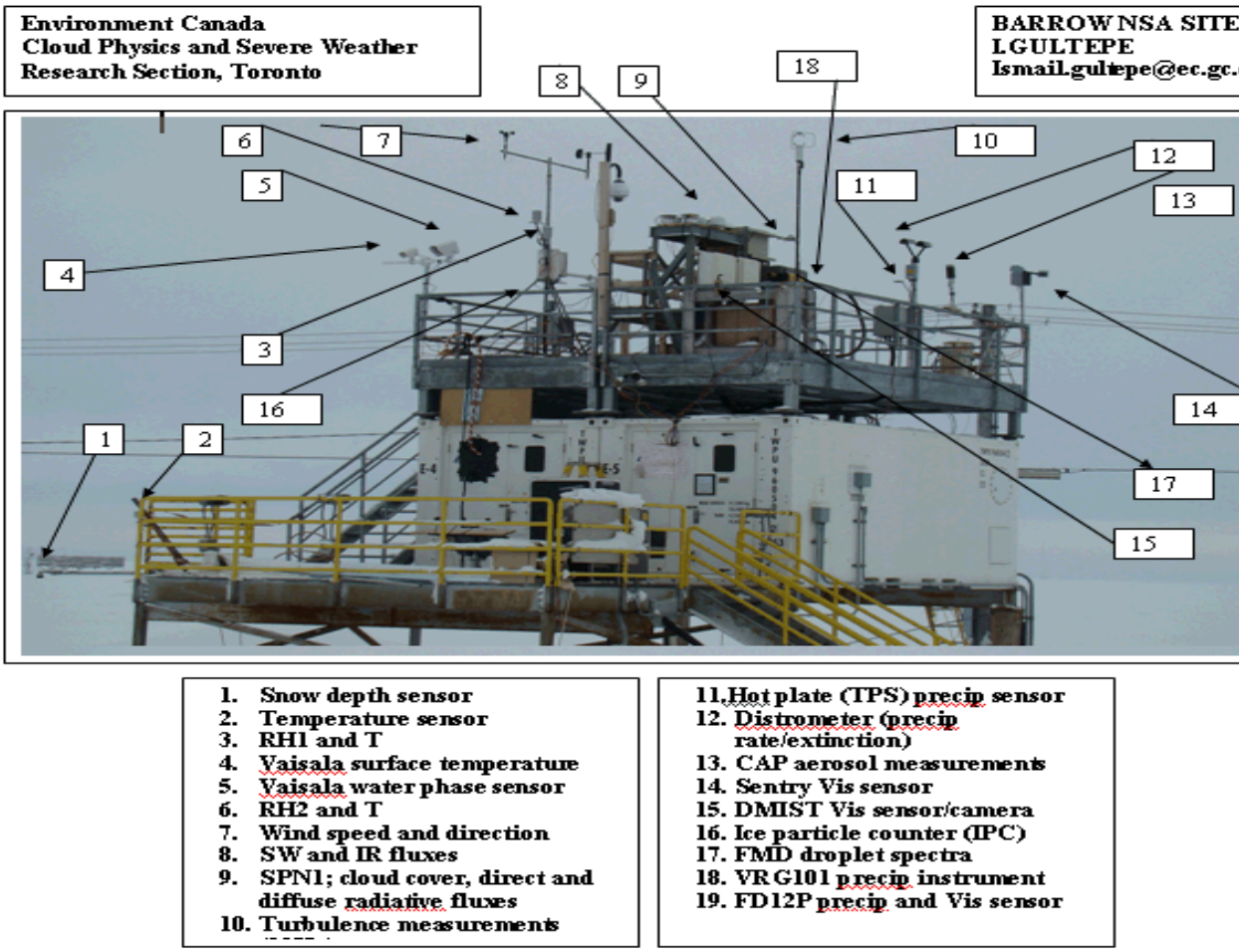

Figure 1: Photograph of the Barrow NSA Site with additional instruments installed for ISDAC labelled and noted in the caption (Photo credit: I. Gultepe).

Figure 2: Photo of NRC Convair-580 taking off from Fairbanks during ISDAC. Multiple probes can be seen hanging from wings (Photo credit: ?)

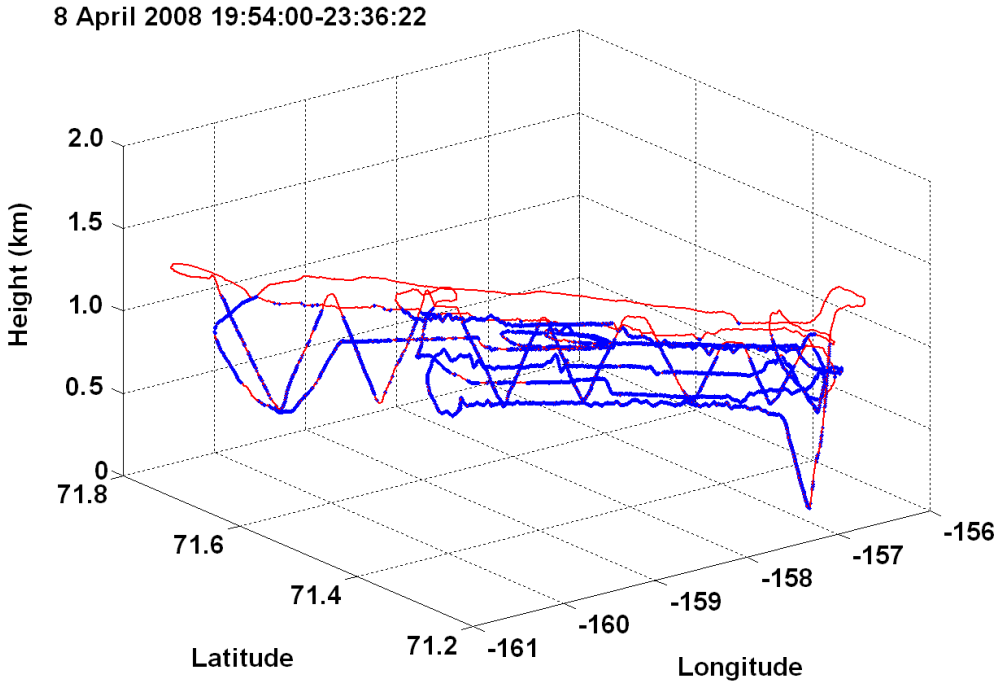

Figure 3: Flight track flown by NRC Convair-580 on Sortie #16, 8 April 2008. Constant altitude flight legs flown above, below and within cloud, together with ramped ascents and descents through cloud and spirals over NSA site. Red represents locations where clouds were sampled, with cloud identified as locations where 10-s averaged CSI total water content > 0.001 g m^{-3}.

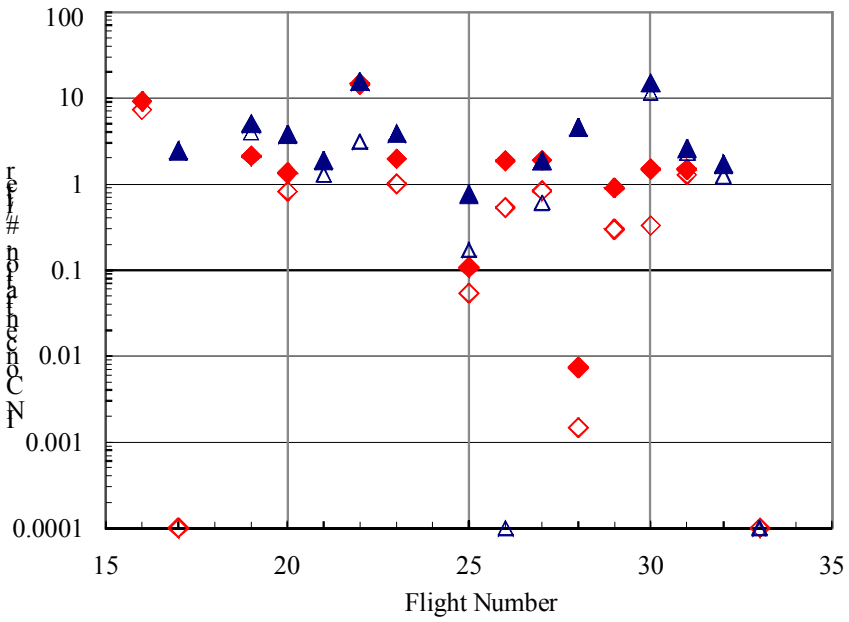

Figure 4: Average IN concentrations measured below (-10 to 0% SS_w) and above water saturation (0 to +10% SS_w) shown as solid diamonds and triangles, respectively, as function of flight number. In addition, lower limits to the IN concentrations below (-10 to 0% SS_w) and above water saturation (0 to +10% SS_w) are shown as open diamonds and triangles, respectively. Data in the figure were collected by sampling on the ambient inlet during clear air conditions.

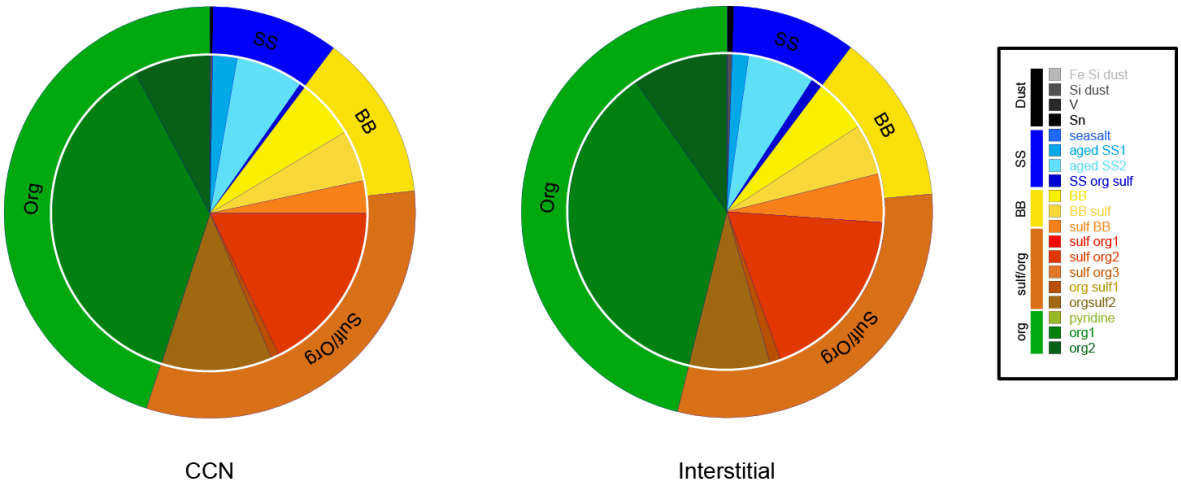

CCN

Interstitial

Figure 5: Pie charts showing the compositions of particles that were activated to form cloud droplets (left) and the composition of particles, in the very same air-mass, that were not activated. Observations acquired on 26 April.

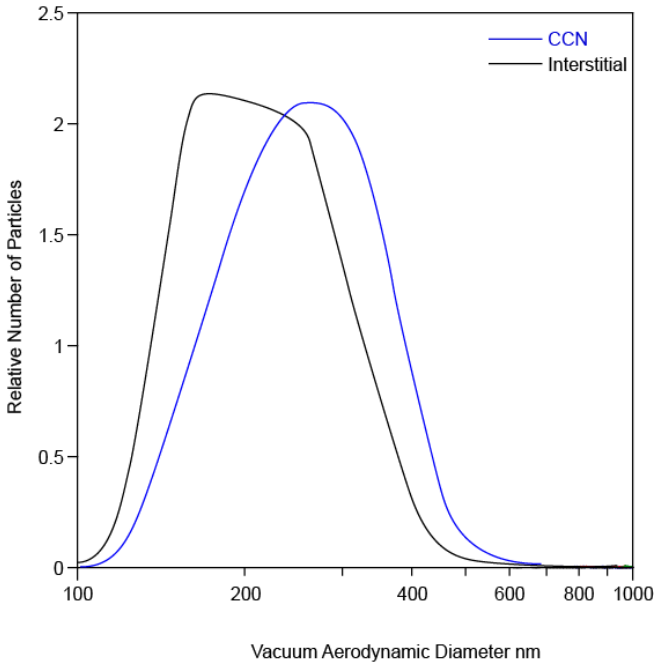

Figure 6: The SPLAT measured size distribution of the particles that activated to form cloud droplets (blue) and of particles that were not activated (black). Observations acquired on 26 April.

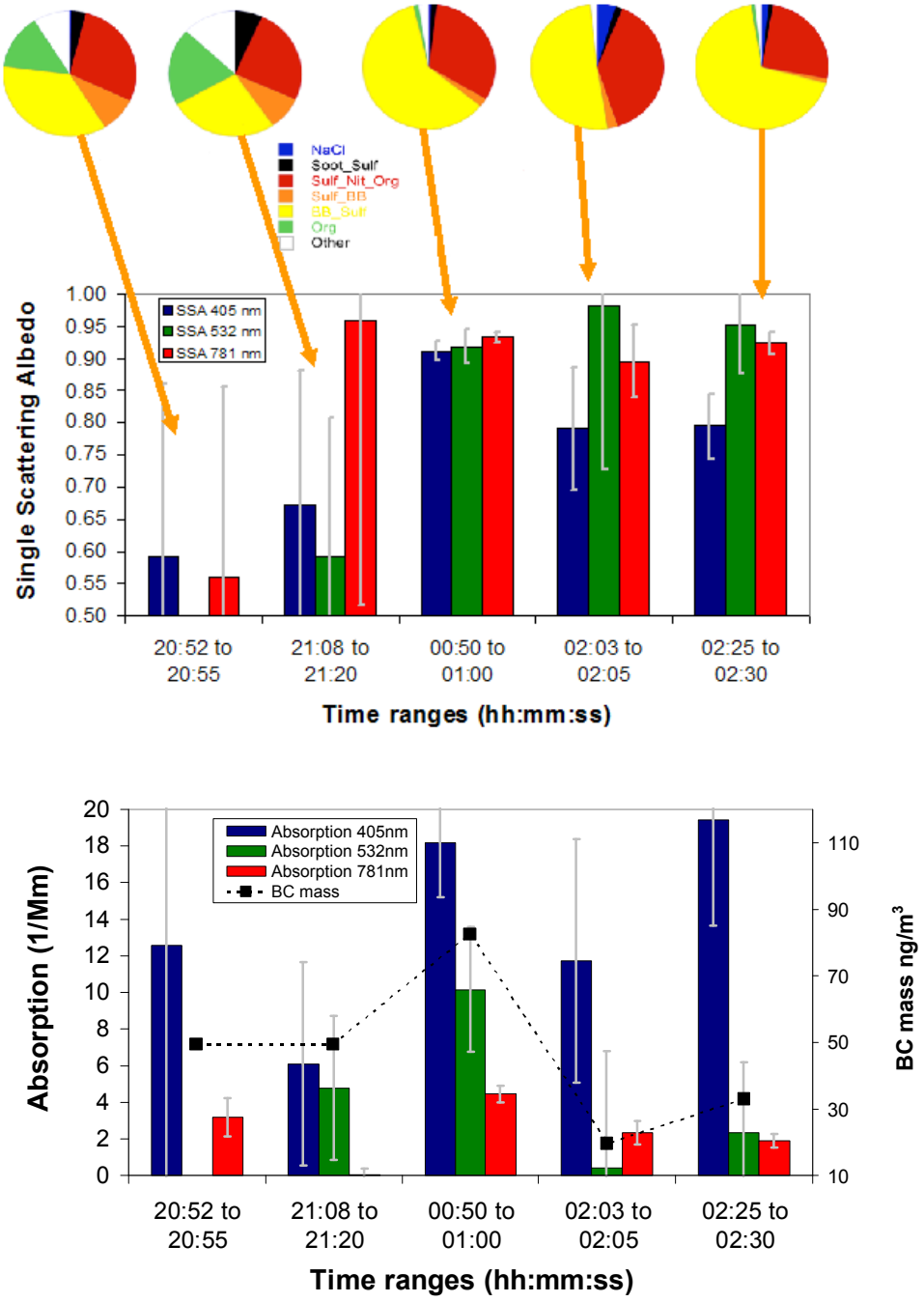

Figure 7: a) Measured ω_0 (780, 532, 405nm) for selected periods on 19 April 2008. Chemical composition of aerosol derived from SPLAT also shown. b) Absorption (left axis) at 3 wavelengths and black carbon mass concentration measured by SPLAT over same time periods contained in particles that are a mixture of soot and sulfate only; this does not include black carbon mass present in biomass burning aerosols seen in pie charts in a.

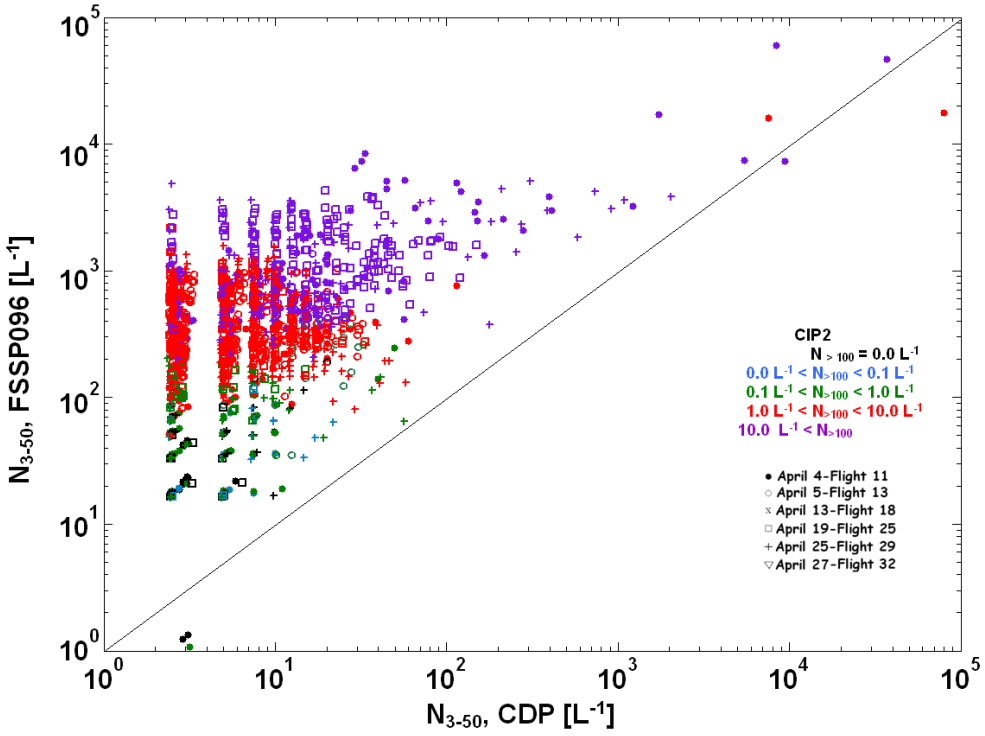

Figure 8: $N_{3\text{-}50,FSSP}$ as function of $N_{3\text{-}50,CDP}$ for measurements made in cirrus during transits between Fairbanks and Barrow on 4, 5, 13, 19 and 25 April 2008. Different dates are indicated by different symbols. Colors indicate different concentration of particles with D > 100 μm measured by the CIP2.

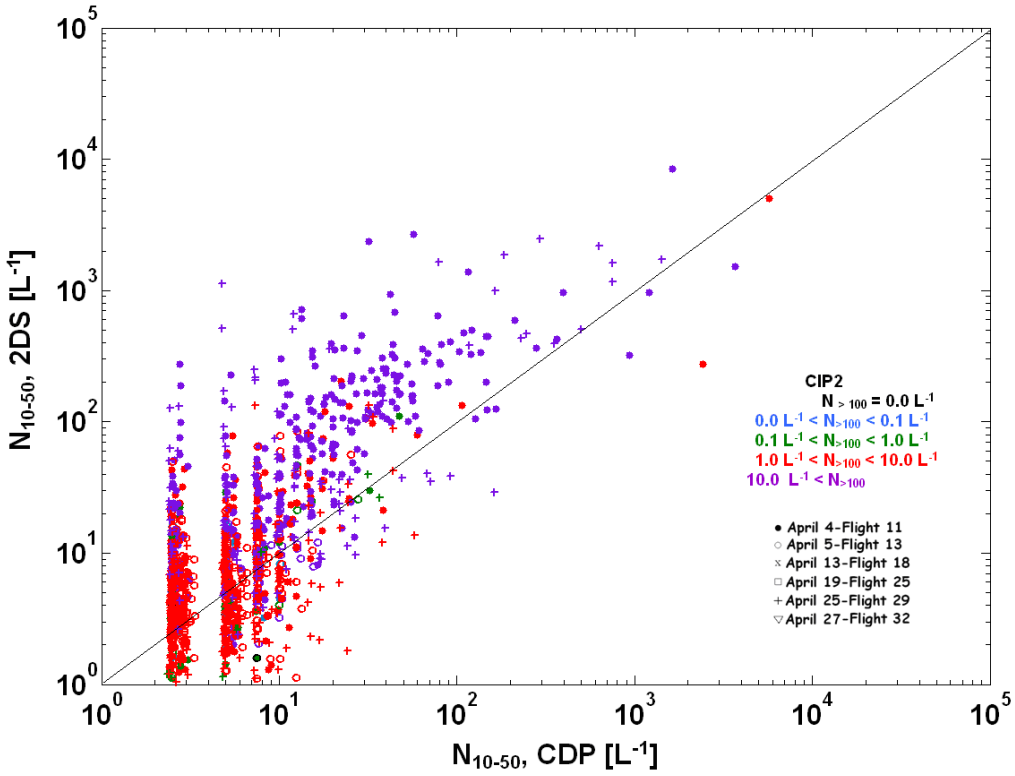

Figure 9: $N_{3\text{-}50,2DS}$ as function of $N_{3\text{-}50,CDP}$ for measurements made in cirrus during transits between Fairbanks and Barrow on 4, 5, 13, 19 and 25 April 2008. Different dates are indicated by different symbols. Colors indicate different concentration of particles with D > 100 μm measured by the CIP2.

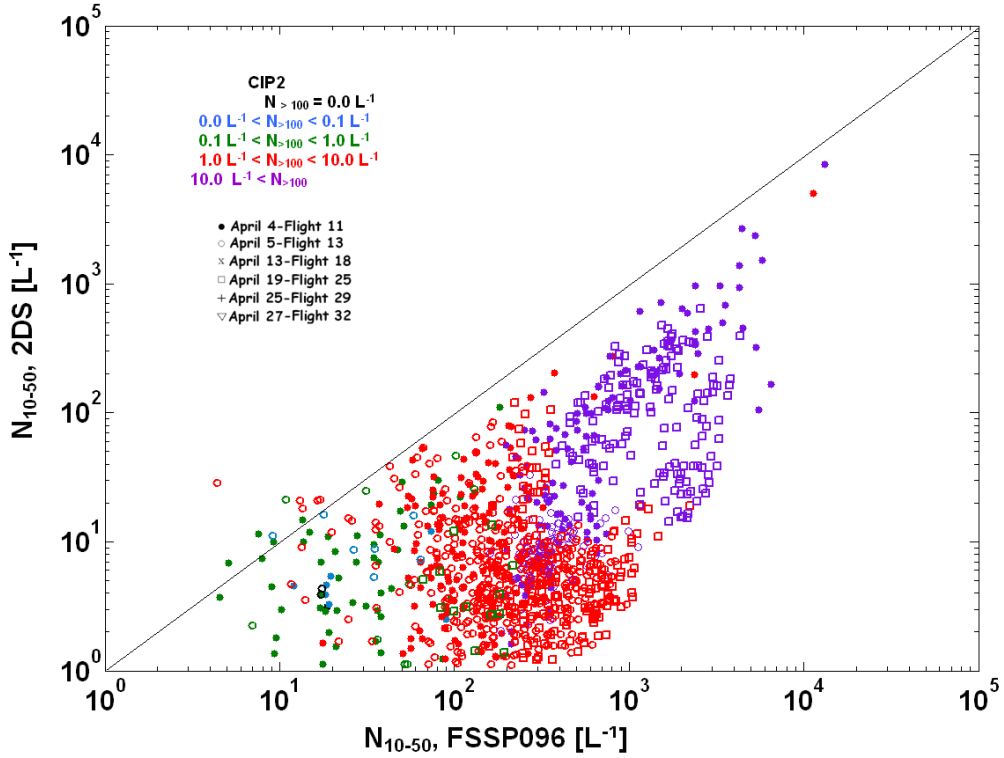

Figure 10: $N_{3\text{-}50,2DS}$ as function of $N_{3\text{-}50,FSSP}$ for measurements made in cirrus during transits between Fairbanks and Barrow on 4, 5, 13, 19 and 25 April 2008. Different dates are indicated by different symbols. Colors indicate different concentration of particles with D > 100 μm measured by the CIP2.

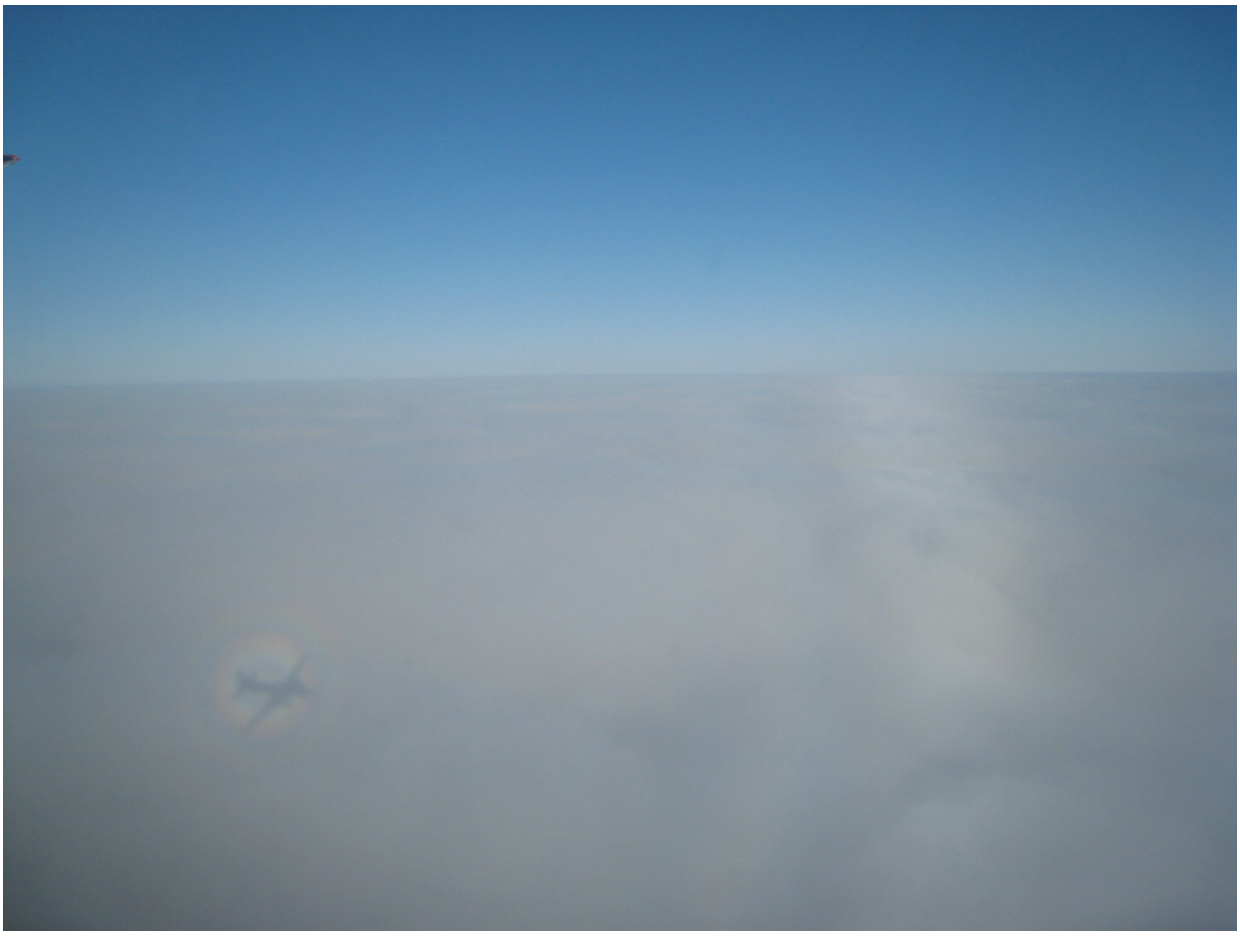

Figure 11: Image of single-layer stratocumulus deck sampled by NRC Convair-580 on 8 Ap1il 2008. Glory and shadow of aircraft are seen in photo. Photo taken by Alexei Korolev when NRC Convair-580 was executing flight leg above deck.

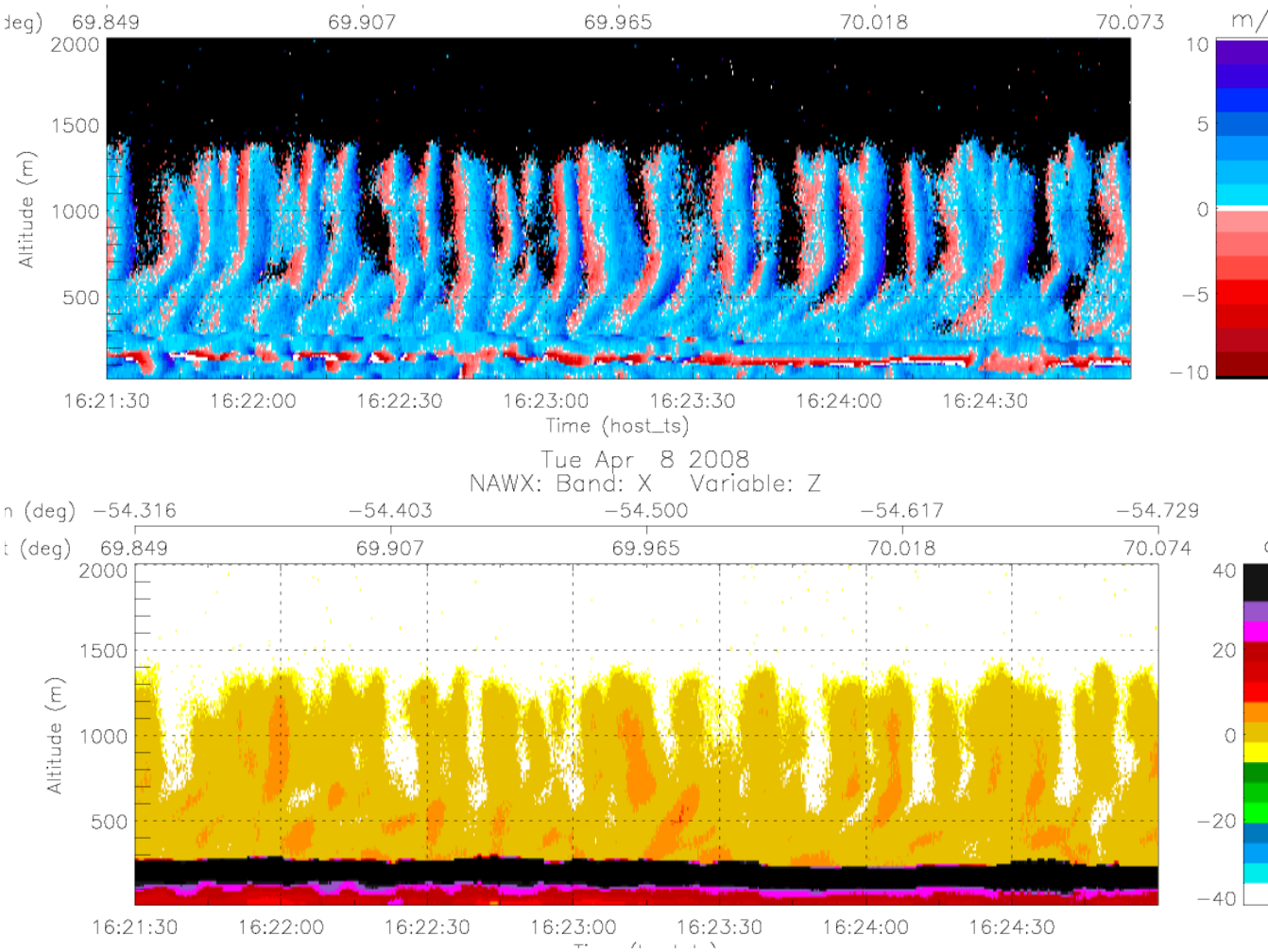

Figure 12: Cross-section of Doppler velocity (V), with negative values indicating upward motion, and reflectivity (Z) measured by NRC X-band radar during constant altitude leg flight above single-layer stratocumulus deck on 8 April 2008.

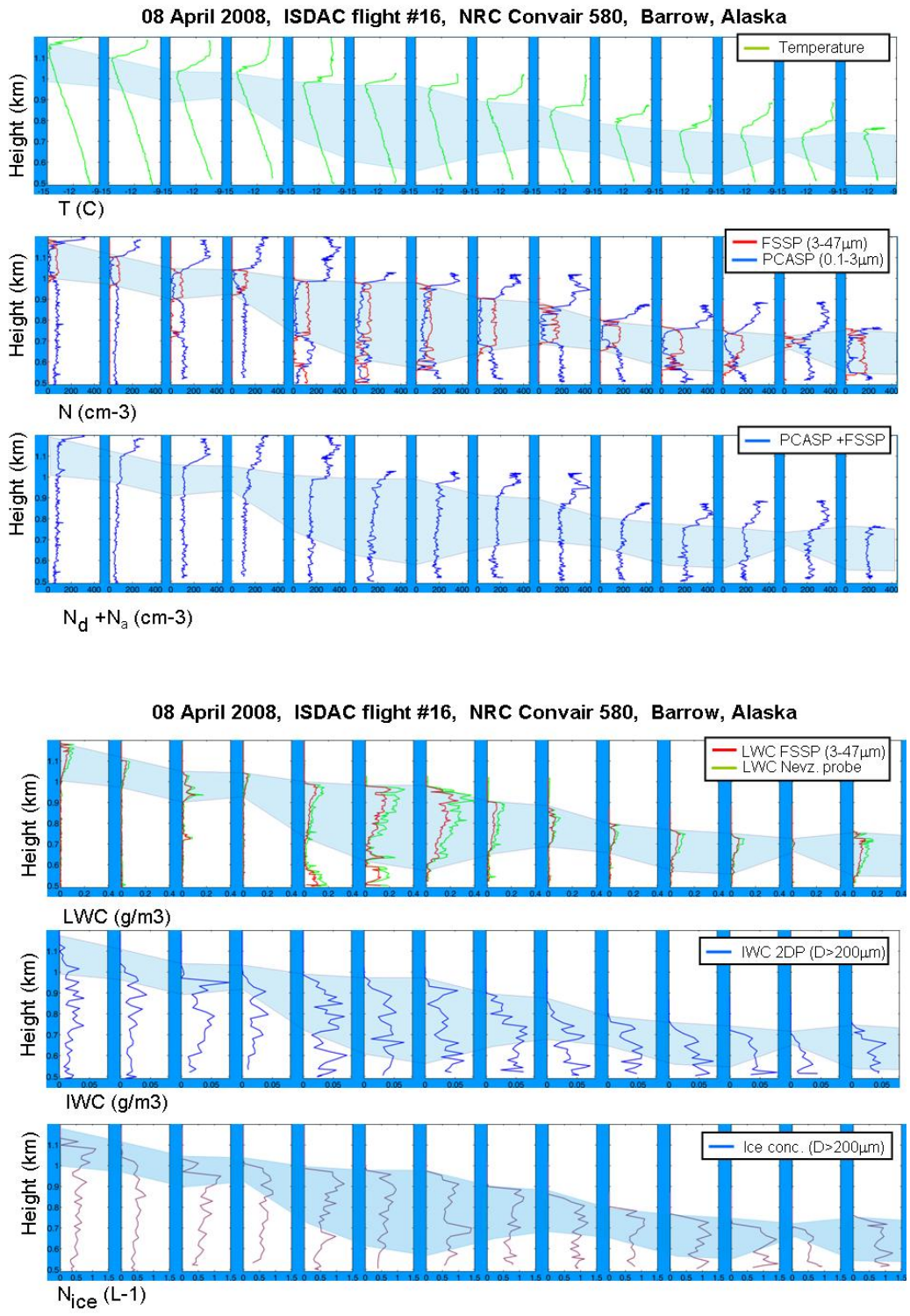

Figure 13: Vertical profile of a) temperature, b) cloud droplet number concentration from FSSP96 (N_d) and aerosol concentration from PCASP (N_a), c) $N_d + N_a$, d) liquid water content derived from FSSP96 size distribution and directly measured by Nevzorov probe, e) ice water content derived from size distribution measured by 2DP, and f) ice crystal concentration derived from 2DP. Each vertical profile was obtained

during a single ramped ascent or descent during the leg when NRC Convair-580 porpoised from cloud top to bottom during Sortie 16 on 8 April 2008. Blue shading, based on analysis of individual profiles, represents location of liquid cloud layer on each profile.

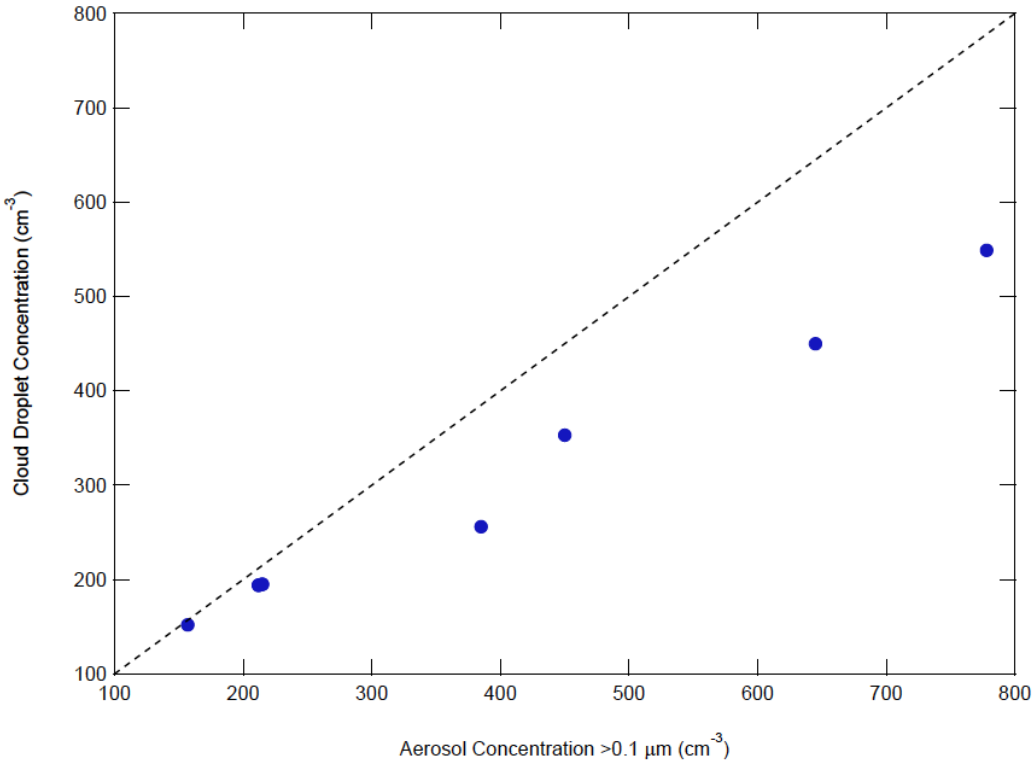

Figure 14: Mean concentrations of cloud droplets and sub-cloud aerosol particles larger than 0.1 µm on 6 different flights during ISDAC.

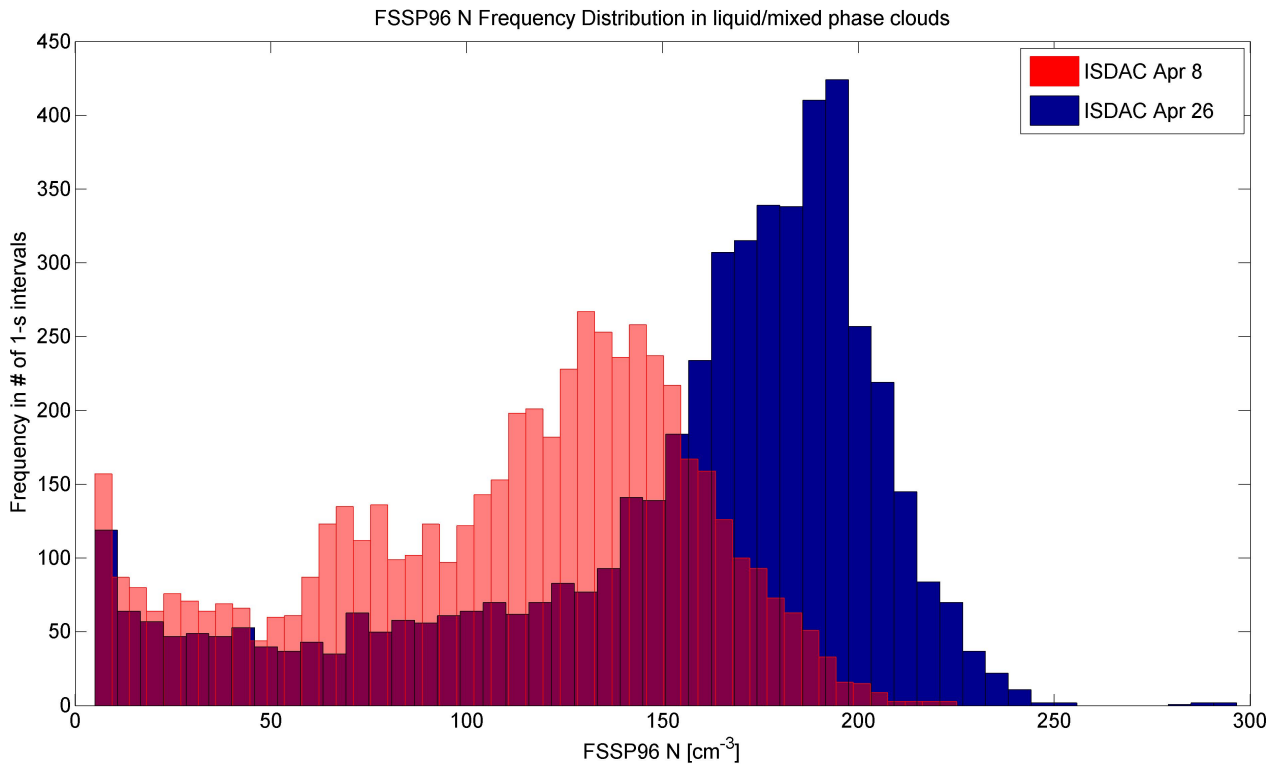

Figure 15: Frequency distribution of number concentration measured by FSSP96 in liquid and mixed-phase clouds for single-layer stratocumulus sampled on 8 and 26 April 2008. Each measurement represents a 1-s average or approximately 120 m of track length.

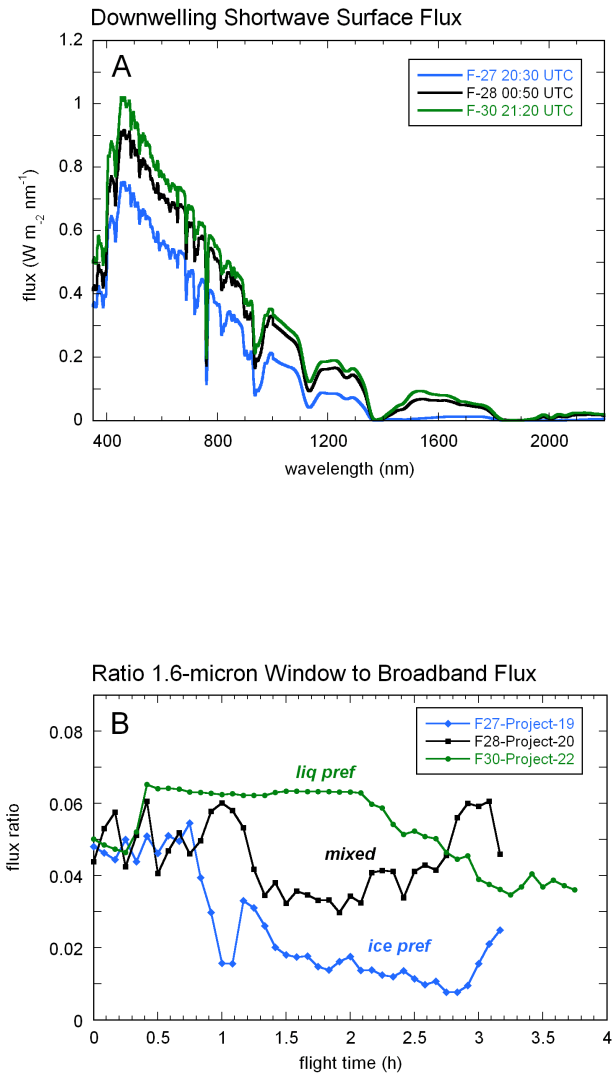

Figure 16. (A) Downwelling surface spectral flux obtained from the ASD (Inc.) spectroradiometer at NSA under flights F-27 and F-28 on 24 April and under flight F-30 on 26 April (F-30), 2008. The spectra were obtained approximately 2.5 hours into each flight. (B) For the duration of these three flights, the ratio of the surface flux in the 1.6 micron window to the broadband flux, in five minute intervals.

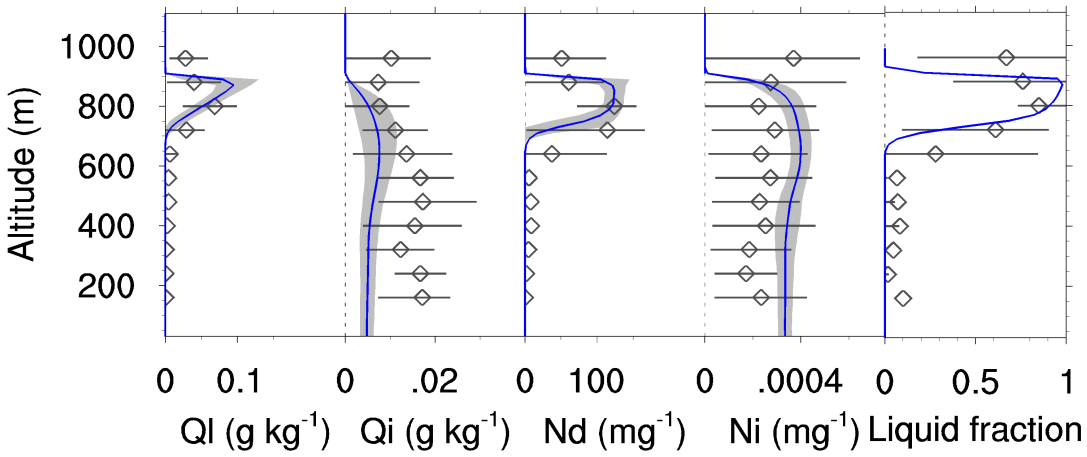

Figure 17: Model predicted (lines) and observed (diamonds) mean vertical profiles of mixed-phase cloud parameters (liquid, Ql, and ice, Qi, mass mixing ratios, droplet, Nd, and ice particle, Ni, number mixing ratios and liquid water condensate fraction) for Sortie # 31 on 26 April 2008. Shaded area and horizontal lines indicate 15 to 85 percentile ranges for simulated and measured parameters, respectively.